Supplementary Figures

Figure S1. Sequence identity assessment: Odin-Sam1 (Homo sapiens) *vs* Odin-Sam1 (Mus musculus)/Ship2-Sam (Homo sapiens)/SASH1-Sam1 (Homo sapiens)/Odin-Sam2 (Homo sapiens).

Figure S2. HOPE analysis of the effect of mutations on structural variation in Odin-Sam1.

Figure S3. MEDUSA analysis of the effect of mutations on the flexibility of Odin-Sam1.

Figure S4. NMR structure of Odin-Sam1 and AF2 models of Odin-Sam1 wild-type and diverse cancer-related point mutants.

Figure S5. AF3 predicted models of Odin-Sam1 diverse variants.

Figure S6. Comparison between AF2 and AF3 models of diverse Odin-Sam1 cancer-related variants.

Figure S7. Comparison between Odin-Sam1 NMR structure (2LMR) and AF2/AF3 (WT) models.

Figure S8. The representative structures, shown as separate models, of Odin-Sam1 domain variants extracted from the MD simulations.

Figure S9. Superposition of the Cα atoms of representative structures extracted from the MD simulations.

Figure S10. MD data of WT and D724N replica simulations.

Figure S11. The Haddock Model of the human EphA2-Sam/Odin-Sam1 complex, the NMR structure of the human EphA2-Sam/Ship2-Sam complex, the SWISS-MODEL (SM) generated structure of the human EphA2-Sam/Odin-Sam1 heterodimer.

Figure S12. Superposition of the backbone atoms between the Haddock model of Odin-Sam1 in complex with EphA2-Sam and the corresponding SWISS-MODEL predicted structure.

Figure S13. Validation of the in silico strategy: the best structure from the Haddock Refinement analysis of the human EphA2-Sam/Odin-Sam1 complex (EphA2-Sam residue range T908-V972/Odin-Sam1 residue range S700-P760) in ribbon drawing.

Figure S14. Validation of the in silico strategy: ribbon representation of the best structure from the Haddock Refinement analysis of the human R957C EphA2-Sam/Odin-Sam1 complex.

Figure S15. Validation of the in silico strategy: the best structure from the Mus Musculus EphA2-Sam/Odin-Sam1 complex (EphA2-Sam residue range T909-V973/Odin-Sam1 residues S716-L775) in ribbon drawing.

Figure S16. Validation of the in silico strategy: ribbon representation of the best structure from the Haddock Refinement analysis of the Mus musculus R958C EphA2-Sam/Odin-Sam1 complex.

Figure S17. Ribbon representation of the best structure from the Haddock Refinement run of the EphA2-Sam/D724N Odin-Sam1 complex starting from the SM prediction of the native EphA2-Sam/Odin-Sam1 heterodimer, and summary of intermolecular interactions by LigPlot+.

Figure S18. Ribbon representation of the best structure from the Haddock Refinement run of the EphA2-Sam/V725L Odin-Sam1 complex (the SM prediction of the native EphA2-Sam/Odin-Sam1 heterodimer was employed as the input structure), and summary of intermolecular interactions by LigPlot+.

Figure S19. Ribbon representation of the best structure from the Haddock Refinement run of the EphA2-Sam/G729R Odin-Sam1 complex (the SM prediction of native EphA2-Sam/Odin-Sam1 heterodimer was employed as input structure), and summary of intermolecular interactions by LigPlot+.

Figure S20. Ribbon representation of the best structure from the Haddock Refinement run of the EphA2-Sam/G729W Odin-Sam1 complex (the SM prediction of native EphA2-Sam/Odin-Sam1 heterodimer was employed as input structure), and summary of intermolecular interactions by LigPlot+.

Figure S21. Ribbon representation of the best structure from the Haddock Refinement run of the EphA2-Sam/N731Y Odin-Sam1 complex (the SM prediction of native EphA2-Sam/Odin-Sam1 heterodimer was employed as input structure), and summary of intermolecular interactions by LigPlot+.

Figure S22. PAE analyses for AF2 and AF3 models of the EphA2-Sam/Odin-Sam1 native complexes.

Figure S23. Comparison between Odin-Sam1/EphA2-Sam SM structure with corresponding AF2 and AF3 predictions and between AF2 and AF3 models of native Odin-Sam1/EphA2-Sam.

Figure S24. Comparison between the Odin-Sam1/EphA2-Sam SM model and its template (PDB entry 2KSO) and between the Odin-Sam1/EphA2-Sam AF2 prediction and the Haddock model of EphA2 in complex with Odin-Sam1.

Figure S25. Ribbon representation of the best structure from the Haddock Refinement analysis (native EphA2-Sam/Odin-Sam1 AF2 models as input) of the EphA2-Sam/Odin-Sam1 complex, and summary of intermolecular interactions by LigPlot+.

Figure S26. Ribbon representation of the best structure from the Haddock Refinement analysis (native EphA2-Sam/Odin-Sam1 AF2 models as input) of the EphA2-Sam/D724N Odin-Sam1 complex, and summary of intermolecular interactions by LigPlot+.

Figure S27. Ribbon representation of the best structure from the Haddock Refinement analysis (native EphA2-Sam/Odin-Sam1 AF2 models as input) of the EphA2-Sam/V725L Odin-Sam1 complex, and summary of intermolecular interactions by LigPlot+.

Figure S28. Ribbon representation of the best structure from the Haddock Refinement analysis (native EphA2-Sam/Odin-Sam1 AF2 models as input) of the EphA2-Sam/D737N Odin-Sam1 complex, and summary of intermolecular interactions by LigPlot+.

```
96.7% identity in 60 residues overlap; Score: 294.0; Gap frequency: 0.0%

Odin-Sam1_Human_UniProtQ92625     700 SVGEWLESIGLQQYESKLLLNGFDDVHFLGSNVMEEQDLRDIGISDPQHRRKLLQAARSL 759
Odin-Sam1_Mouse_UniProtP59672     716 SVGEWLESIGLQQYESKLLLNGFDDVRFLGSNVMEEQDLREIGISDPQHRRKLLQAARSL 775
                                      ************************* ************* ******************


48.0% identity in 50 residues overlap; Score: 121.0; Gap frequency: 4.0%

Odin-Sam1_Human_UniProtQ92625         704 WLESIGLQQYESKLLLNGFDDVHFLGSNVMEEQDLRDIGISDPQHRRKLL 753
Ship2-Sam_Human_UniProtO15357        1204 WLRAIGLERYEEGLVHNGWDDLEFLSD--ITEEDLEEAGVQDPAHKRLLL 1251
                                          **  ***  **  *  ** **  **      * **   *  ** * * **


36.7% identity in 60 residues overlap; Score: 93.0; Gap frequency: 3.3%

Odin-Sam1_Human_UniProtQ92625     700 SVGEWLESIGLQQYESKLLLNGFDDVHFLGSNVMEEQDLRDIGISDPQHRRKLLQAARSL 759
SASH1-Sam1_Human_UniProtO94885    637 SVEDLLDRINLKEHMPTFLFNGYEDLDTF--KLLEEEDLDELNIRDPEHRAVLLTAVELL 694
                                      **   *  * *       * **  *         ** **    * ** **  ** *   *


27.8% identity in 54 residues overlap; Score: 64.0; Gap frequency: 1.9%

Odin-Sam1_Human_UniProtQ92625     700 SVGEWLESIGLQQYESKLLLNGFDDVHFLGSNVMEEQDLRDIGISDPQHRRKLL 759
Odin-Sam2_Human_UniProtQ92625     774 SVPSWLDSLGLQDYVHSFLSSGYSSIDTV-KNLWELELVNVLKVQLLGHRKRII 826
                                      **  ** * *** *    *  *         *  *            **
```

Figure S1. Sequence alignment and percentage of sequence identity evaluated through the SIM – Alignment Tool [1] of EXPASY [2] (https://web.expasy.org/sim/, access date 6 October 2025): Odin-Sam1 (Homo sapiens) sequence was compared with 1) Odin-Sam1 (Mus musculus) / 2) Ship2-Sam (Homo sapiens) / 3) SASH1-Sam1 (Homo sapiens) / 4) Odin-Sam2 (Homo sapiens).



Amino Acid Properties
- The wild-type and mutant amino acids differ in size.
- The mutant residue is bigger, this might lead to bumps.
- The hydrophobicity of the wild-type and mutant residue differs.
- The mutation introduces a more hydrophobic residue at this position. This can result in loss of hydrogen bonds and/or disturb correct folding.



Amino Acid Properties
- The wild-type and mutant amino acids differ in size.
- The mutant residue is smaller, this might lead to loss of interactions.



Amino Acid Properties
- There is a difference in charge between the wild-type and mutant amino acid.
- The mutation introduces a residue with a charge opposite to the wild-type. This can cause repulsion with other residues in the protein or ligands.
- The wild-type and mutant amino acids differ in size.
- The mutant residue is bigger, this might lead to bumps.



Amino Acid Properties
- The wild-type and mutant amino acids differ in size.
- The mutant residue is bigger, this might lead to bumps.



Amino Acid Properties
- There is a difference in charge between the wild-type and mutant amino acid.
- The charge of the wild-type residue will be lost, this can cause loss of interactions with other molecules or residues.



Amino Acid Properties
- The wild-type and mutant amino acids differ in size.
- The mutant residue is bigger, this might lead to bumps.

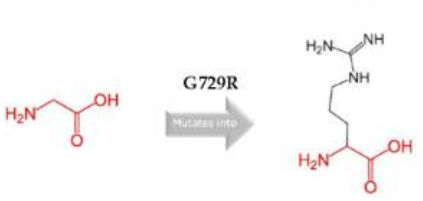

Amino Acid Properties
- There is a difference in charge between the wild-type and mutant amino acid.
- The mutation introduces a charge, this can cause repulsion of ligands or other residues with the same charge.
- The wild-type and mutant amino acids differ in size.
- The mutant residue is bigger, this might lead to bumps.
- The torsion angles for this residue are unusual; only glycine is flexible enough to make these torsion angles, mutation into another residue will force the local backbone into an incorrect conformation and will disturb the local structure.



Amino Acid Properties
- The wild-type and mutant amino acids differ in size.
- The mutant residue is bigger, this might lead to bumps.
- The torsion angles for this residue are unusual; only glycine is flexible enough to make these torsion angles, mutation into another residue will force the local backbone into an incorrect conformation and will disturb the local structure.



Amino Acid Properties
- The wild-type and mutant amino acids differ in size.
- The mutant residue is bigger, this might lead to bumps.
- The hydrophobicity of the wild-type and mutant residue differs.
- The mutation introduces a more hydrophobic residue at this position. This can result in loss of hydrogen bonds and/or disturb correct folding.



Amino Acid Properties
- There is a difference in charge between the wild-type and mutant amino acid.
- The charge of the wild-type residue will be lost, this can cause loss of interactions with other molecules or residues.



Amino Acid Properties
- There is a difference in charge between the wild-type and mutant amino acid.
- The charge of the wild-type residue will be lost, this can cause loss of interactions with other molecules or residues.

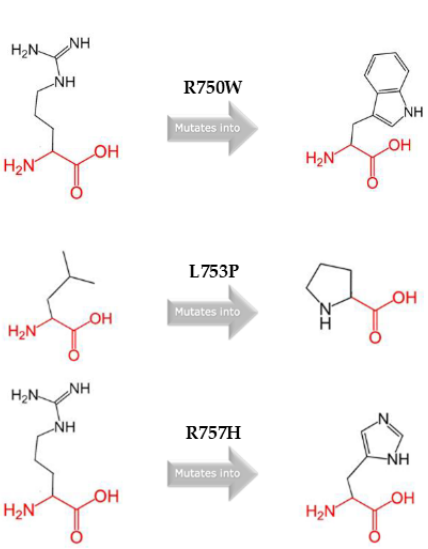

Amino Acid Properties

- There is a difference in charge between the wild-type and mutant amino acid.
- The charge of the wild-type residue will be lost, this can cause loss of interactions with other molecules or residues.
- The wild-type and mutant amino acids differ in size.
- The mutant residue is bigger, this might lead to bumps.
- The hydrophobicity of the wild-type and mutant residue differs.
- The mutation introduces a more hydrophobic residue at this position. This can result in loss of hydrogen bonds and/or disturb correct folding.

Amino Acid Properties

- The wild-type and mutant amino acids differ in size.
- The mutant residue is smaller, this might lead to loss of interactions.

Amino Acid Properties

- There is a difference in charge between the wild-type and mutant amino acid.
- The charge of the wild-type residue will be lost, this can cause loss of interactions with other molecules or residues.
- The wild-type and mutant amino acids differ in size.
- The mutant residue is smaller, this might lead to loss of interactions.

Figure S2. HOPE analysis [3] of the effect of mutations on structural variation in Odin-Sam1 in terms of size, charge, hydrophobicity, and spatial structure compared to the wild type.

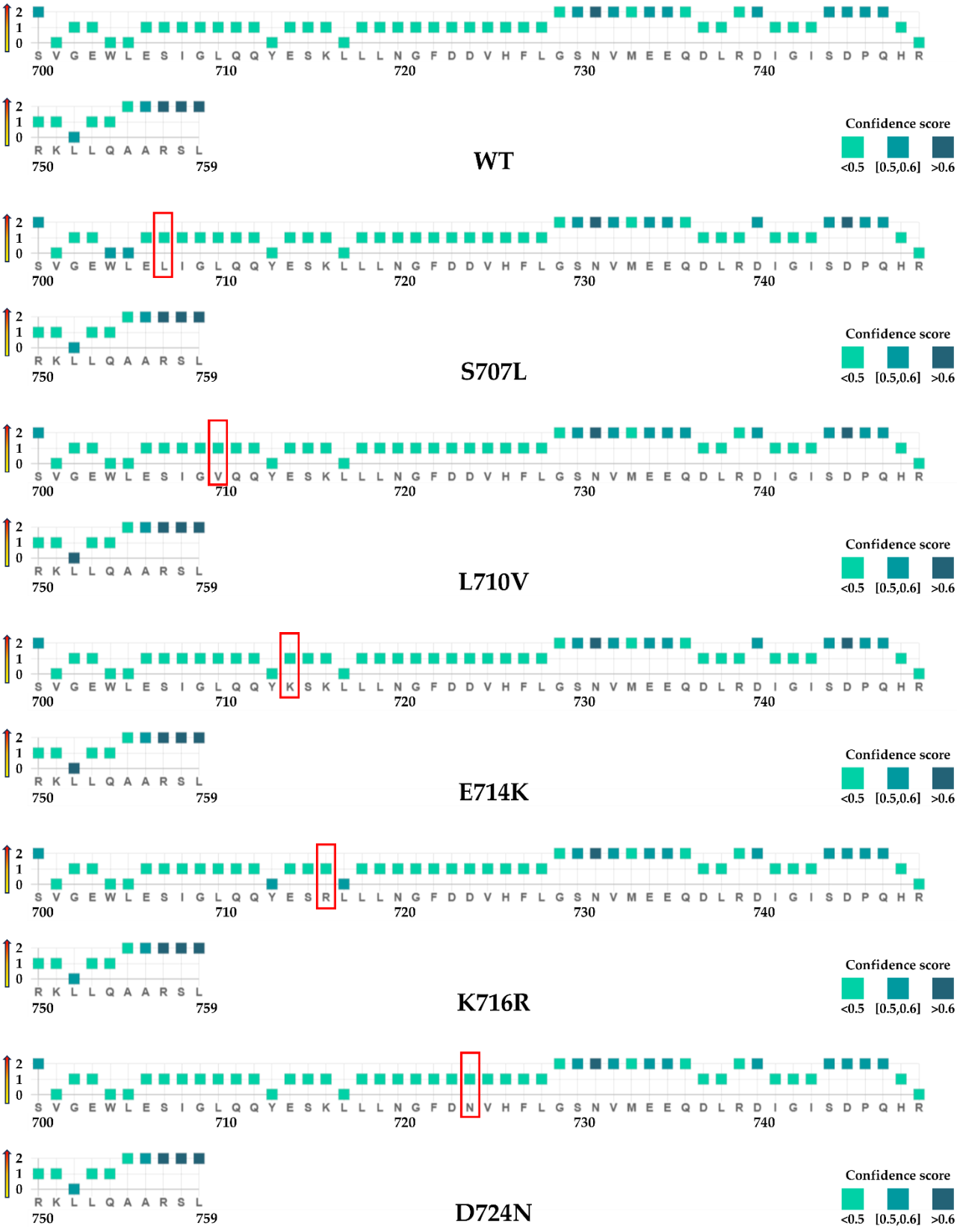
WT
S707L
L710V
E714K
K716R
D724N
Confidence score
<0.5
[0.5,0.6]
>0.6

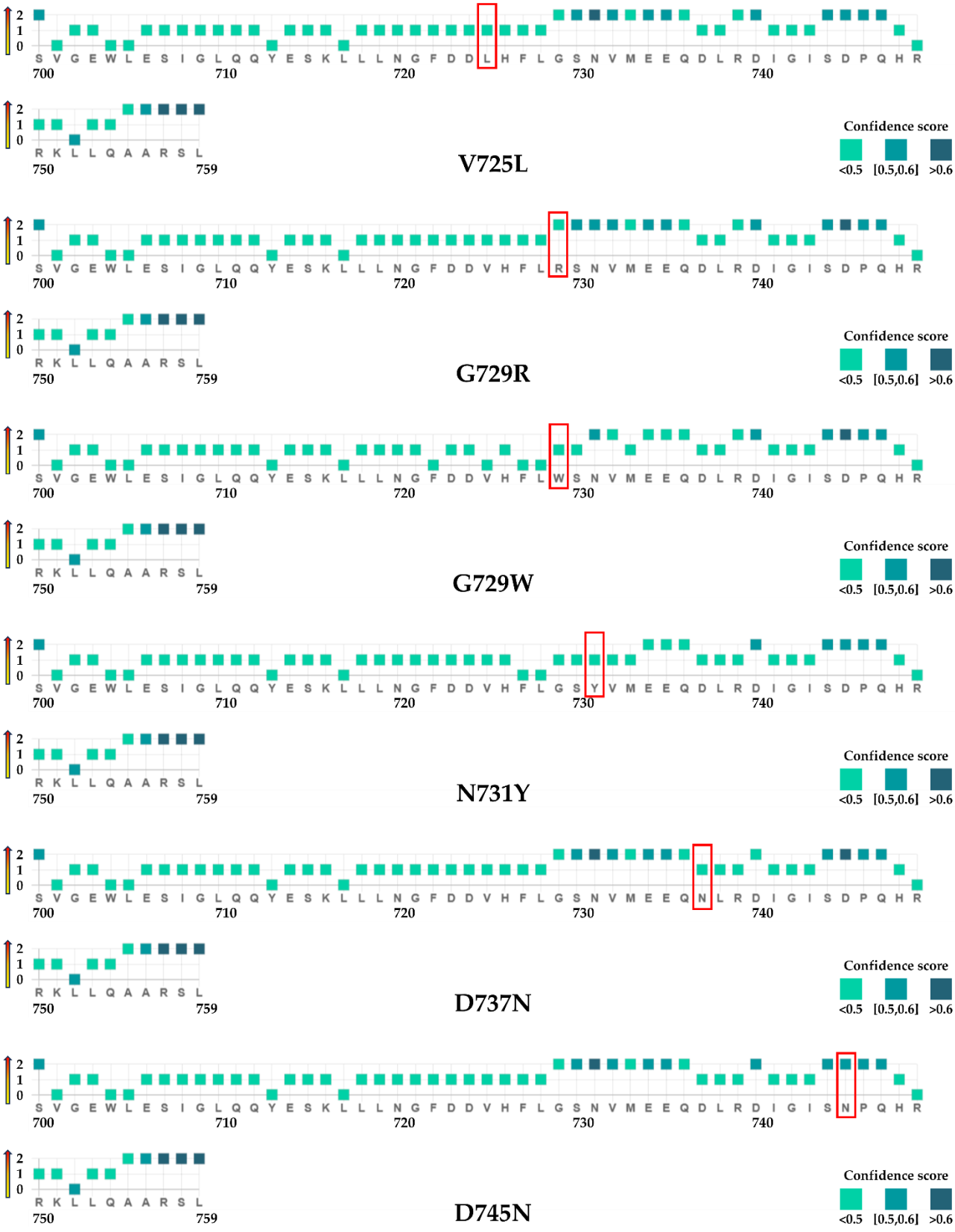
2
1
0
S V G E W L E S I G L Q Q Y E S K L L L N G F D D L H F L G S N V M E E Q D L R D I G I S D P Q H R
700
710
720
730
740
R K L L Q A A R S L
750
759
V725L
G729R
G729W
N731Y
D737N
D745N
Confidence score
<0.5
[0.5,0.6]
>0.6

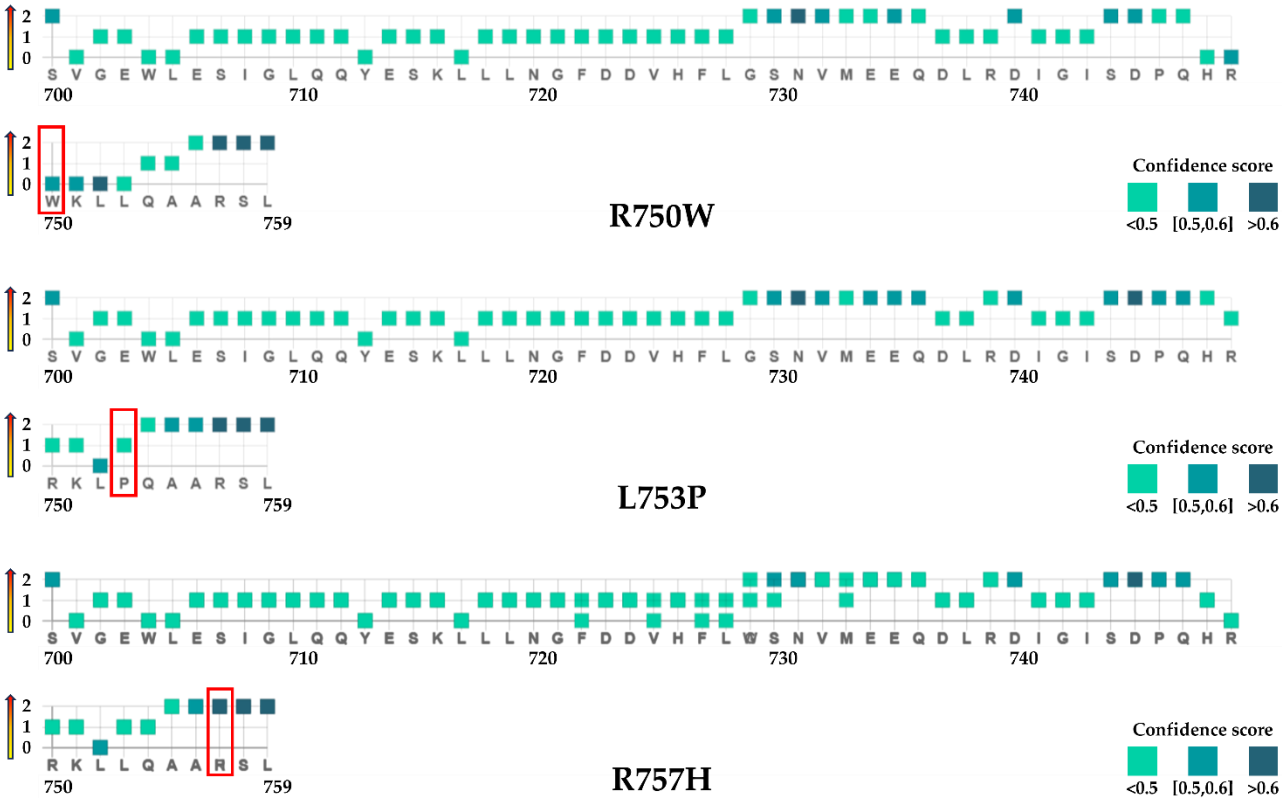

Figure S3. MEDUSA analysis [4] to predict the effect of cancer-related mutations on Odin-Sam1 flexibility. The arrow direction, on the left-side of each diagram, points towards increased flexibility. Confidence scores are shown on the right side, with darker squares indicating improved confidence level. Mutations are enclosed in red boxes.

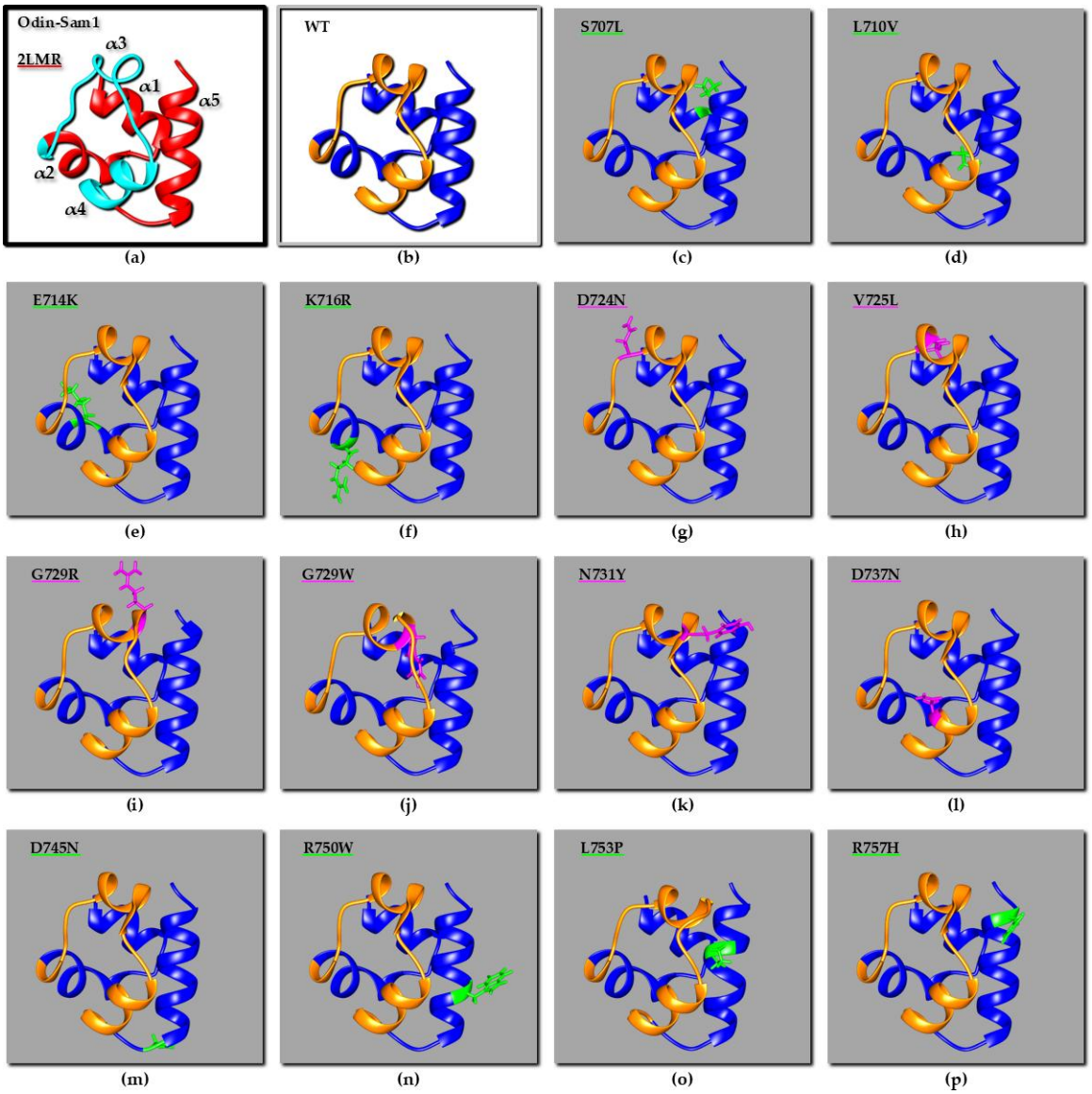

Figure S4. (**a**) NMR Structure of Odin-Sam1 (first conformer -residues S700-L759, pdb entry 2LMR [5] after removal of the flexible N- and C-tails, 3 cycles of the FoldX RepairPDB macro [6] and the addition of protons by UCSF Chimera (v. 1.20) [7]) in a ribbon representation (red). AF2 [8, 9] models of (**b**) Odin-Sam1 wild-type and cancer-related mutants (**c**) S707L, (**d**) L710V, (**e**) E714K, (**f**) K716R, (**g**) D724N, (**h**) V725L, (**i**) G729R, (**j**) G729W, (**k**) N731Y, (**l**) D737N, (**m**) D745N, (**n**) R750W, (**o**) L753P, (**p**) R757H. The mutated residues in cancer are highlighted in green (if located outside of the ML) and magenta (if located within the ML) on the ribbon representations in (**c-p**). The ML Interface (residues L719-G742) is colored in cyan (**a**) and orange in (**b-p**). Only the best predicted AF2 models are shown.

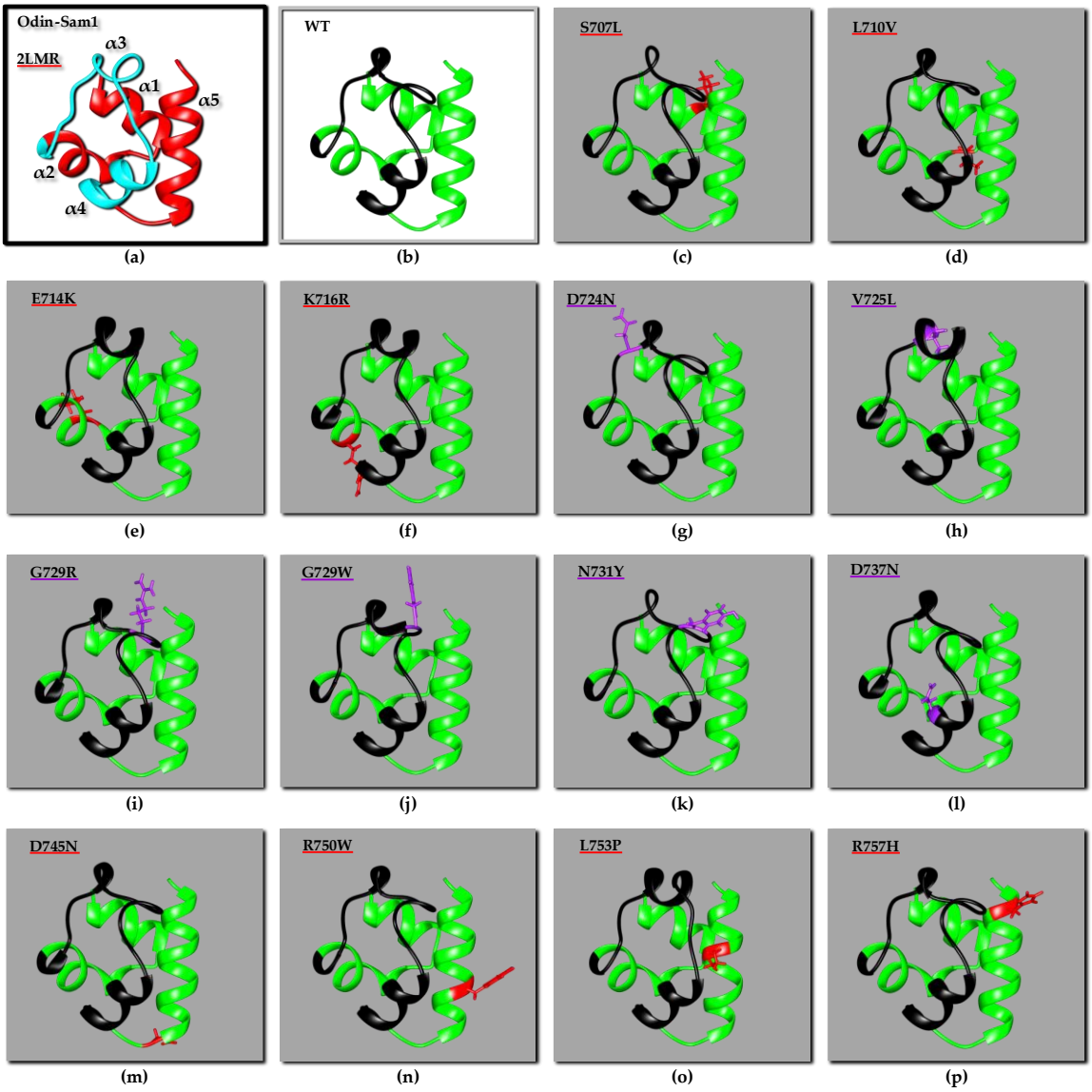

Figure S5. (**a**) NMR Structure of Odin-Sam1 (first conformer -residues S700-L759, pdb entry 2LMR [5] after removal of the flexible N- and C-tails, 3 cycles of the FoldX RepairPDB macro [6] and the addition of protons by UCSF Chimera (v. 1.20) [7]) in a ribbon representation (red). AF3 [10] models of (**b**) Odin-Sam1 wild-type and cancer-related mutants (**c**) S707L, (**d**) L710V, (**e**) E714K, (**f**) K716R, (**g**) D724N, (**h**) V725L, (**i**) G729R, (**j**) G729W, (**k**) N731Y, (**l**) D737N, (**m**) D745N, (**n**) R750W, (**o**) L753P, (**p**) R757H. The mutated residues in cancer are highlighted in red (if located outside of the ML) and purple (if located within the ML) on the ribbon representations in (**c-p**). The ML Interface (residues L719-G742) is colored in cyan (**a**) and black in (**b-p**). Only the best predicted AF3 models are shown.

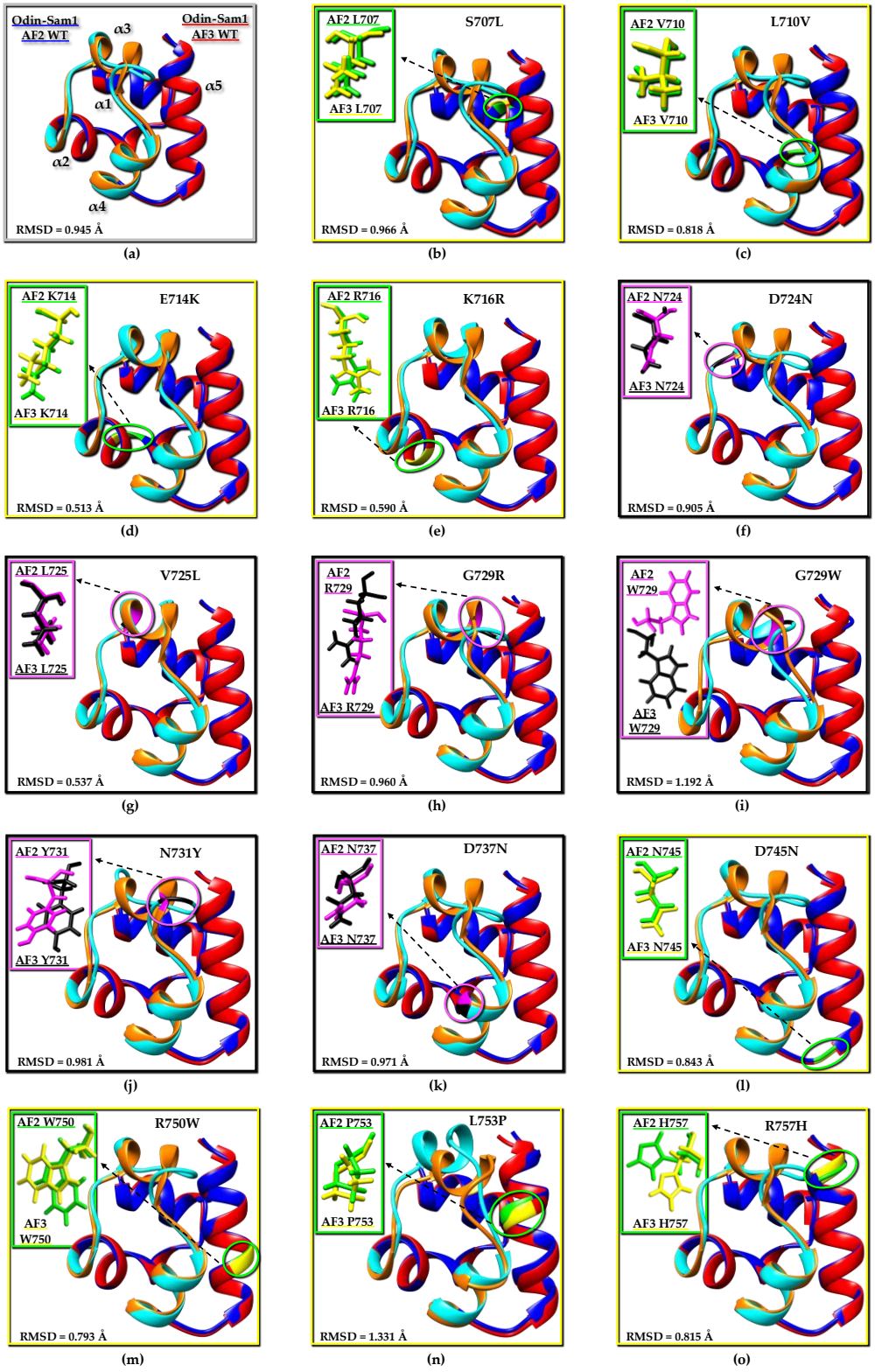

Figure S6. Overlays on the backbone atoms of the Odin-Sam1 AF2 [8, 9](blue) and AF3 [10] (red) models of WT **(a)** and cancer-related mutants: **(b)** S707L, **(c)** L710V, **(d)** E714K, **(e)** K716R, **(f)** D724N, **(g)** V725L, **(h)** G729R, **(i)** G729W, **(j)** N731Y, **(k)** D737N, **(l)** D745N, **(m)** R750W, **(n)** L753P, **(o)** R757H. The ML region (residues L719-G742) is colored in orange and cyan in the AF2 and AF3 models, respectively; the mutations are shown in green (AF2 models) or in yellow (AF3 models) when outside the ML, and in magenta (AF2 models) or in black (AF3 models) when inside the ML and highlighted by colored circles. For a better visualization, the mutated residues in the upper left insets are oriented differently with respect to the backbone overlays shown in the main panels. RMSD values are also reported in each panel.

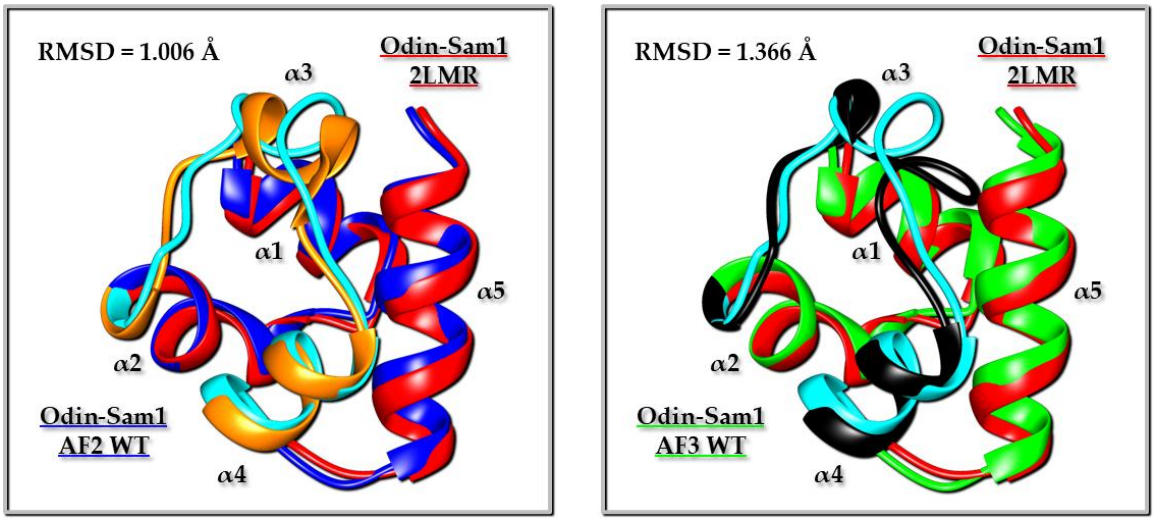

Figure S7. Overlays on the backbone atoms of the Odin-Sam1 NMR structure (first conformer -residues S700-L759-, PDB entry 2LMR [5] after removal of the flexible N- and C-tails, 3 cycles of the FoldX RepairPDB macro [6] and the addition of protons by UCSF Chimera (v. 1.20) [7]) (red in both panels) and AF2 [8, 9] (blue in left panel) or AF3 [10] (green in right panel) models of WT Odin-Sam1. The ML region of Odin-Sam1 (residues L719-G742) is colored in cyan, orange and black in the 2LMR, AF2 and AF3 structures, respectively. RMSD values are also indicated.

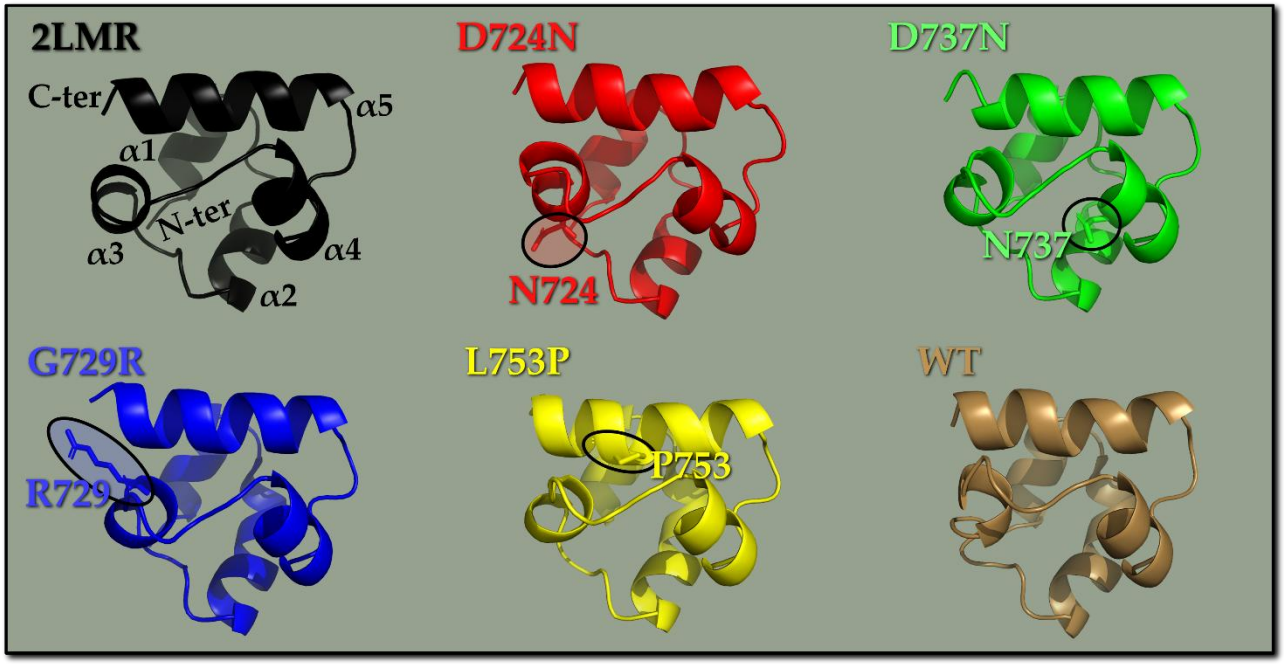

(a)

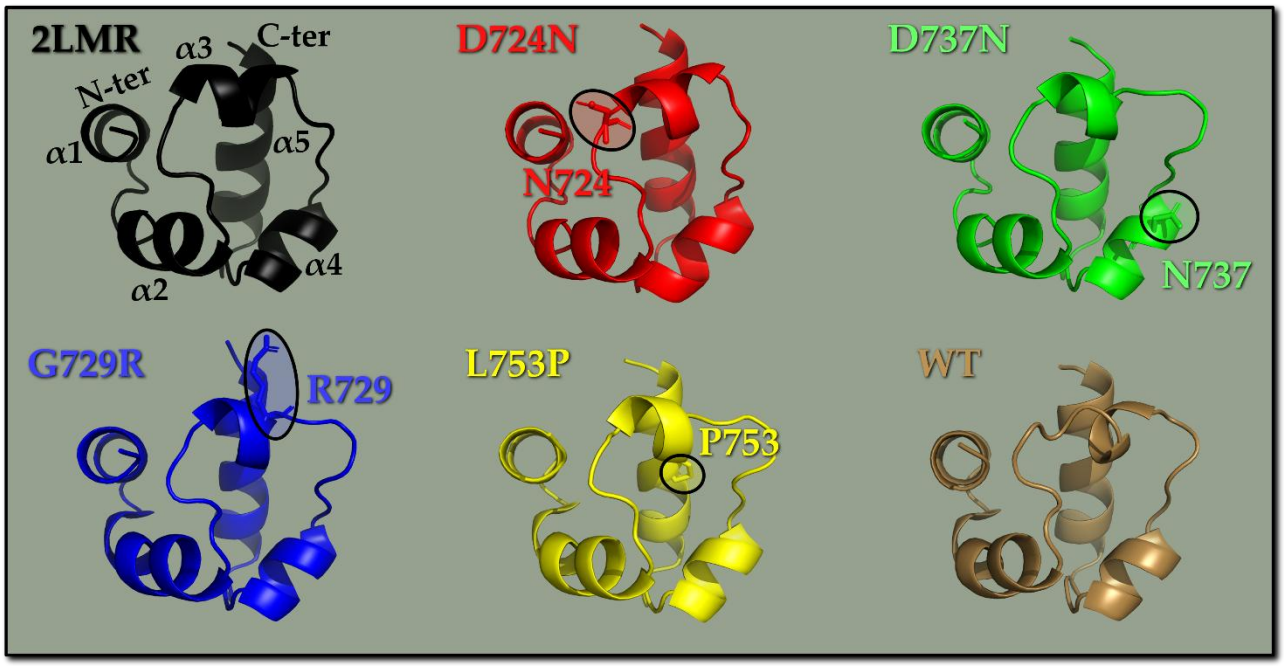

(b)

Figure S8. (a, b) The representative structures of Odin-Sam1 domain variants extracted from the MD simulations are shown as separate models in two diverse orientations. Odin-Sam1 variants are shown in cartoon representation with the following color scheme: black for 2LMR, sand for WT, red for D724N, blue for G729R, green for D737N and yellow for L753P. The side chains of mutated residues are reported in stick and highlighted by circles.

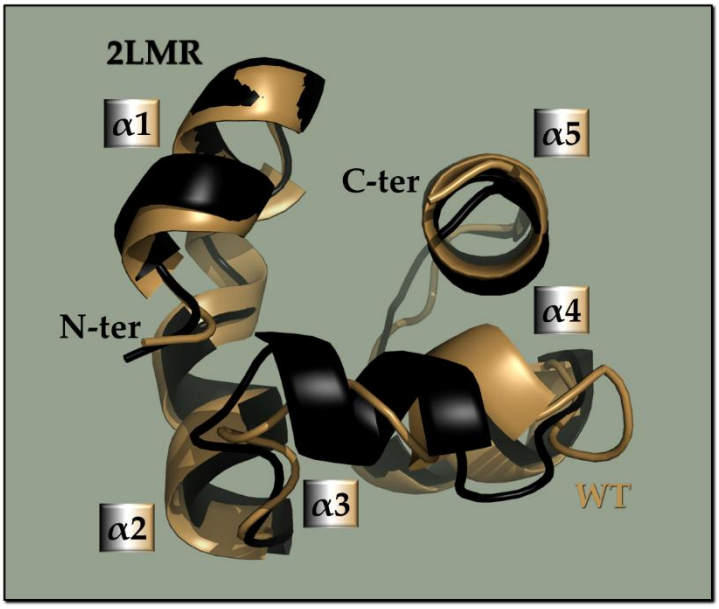

Figure S9. Overlay of the Cα atoms between the representative structures extracted from the MD simulation of "2LMR" (black) and "WT" (sand).

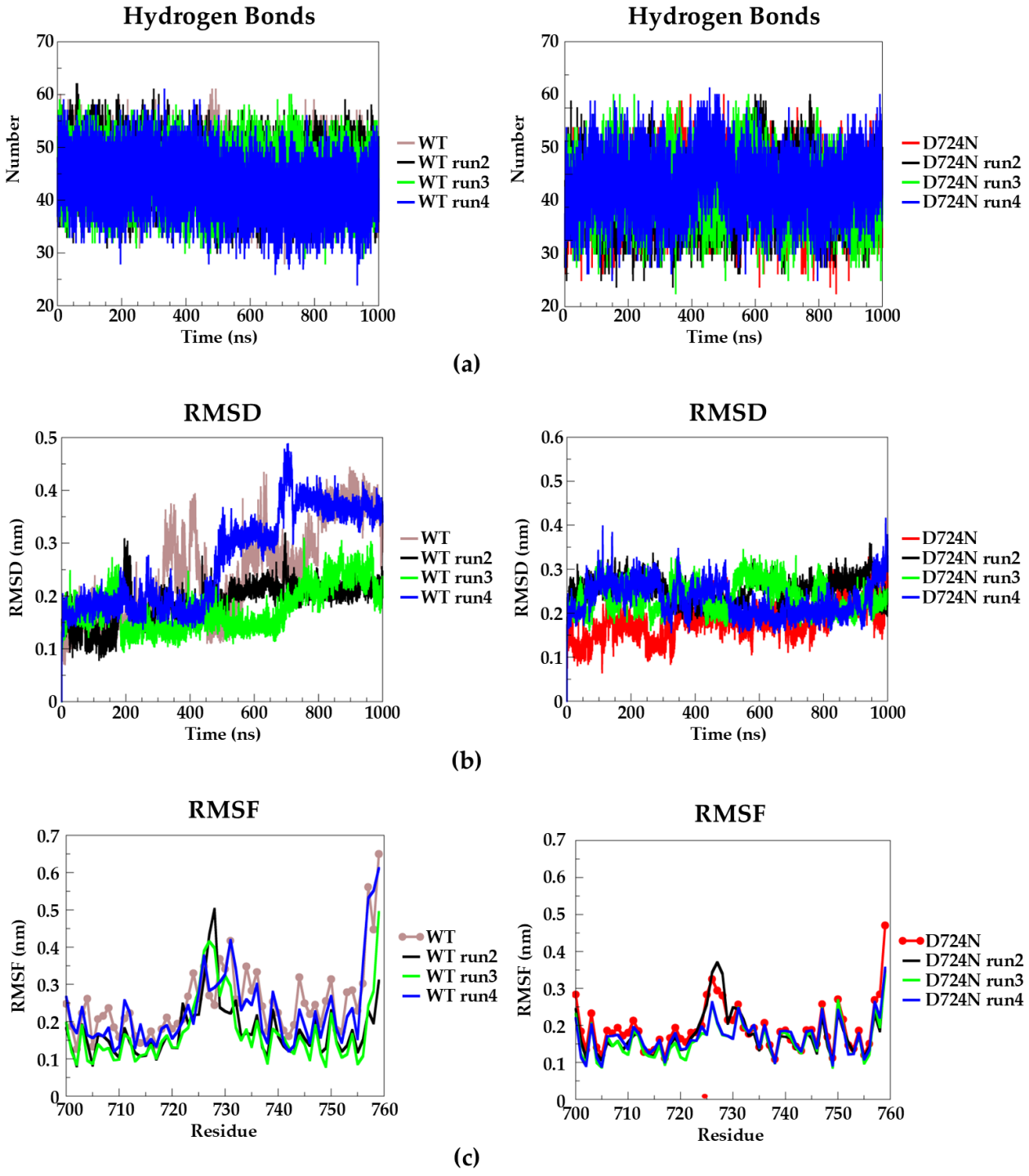

Figure S10. Molecular dynamics studies: ensemble of parameters derived from WT **(a-c, left panels)** and D724N **(a-c, right panels)** replica simulations. **(a)** Number of H-bonds within each system computed along the MD simulations. **(b)** Residue RMSD profiles along the MD simulations, calculated considering the Cα atoms. **(c)** Residue RMSF profiles along the MD simulations. In **(c)** right panel, the red dot on the RMSF graph "Residue" axis indicates the position of the mutation along the Odin-Sam1 sequence.

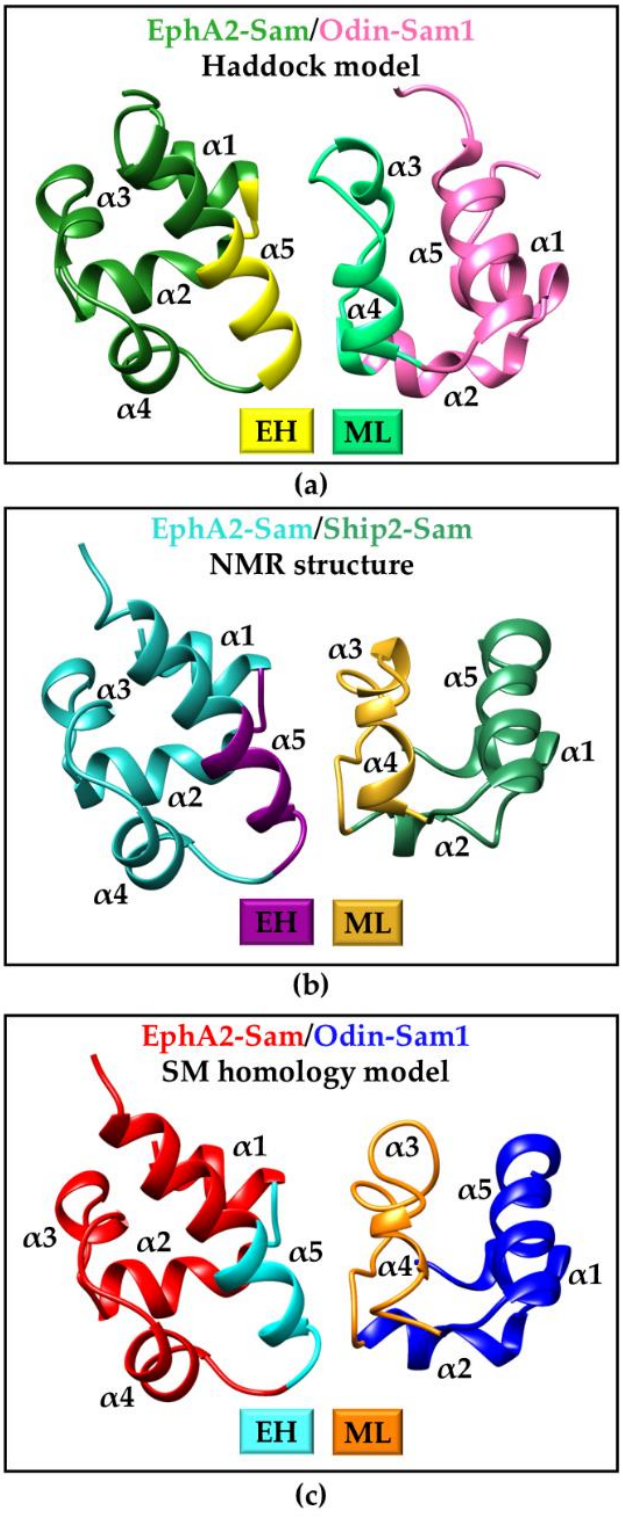

Figure S11. (a) Second best Haddock model of the human EphA2-Sam (forest green)/Odin-Sam1 (pink) complex [5]. **(b)** The NMR solution structure of the human EphA2-Sam (cyan)/Ship2-Sam (sea green) complex (pdb id 2KSO [11], first conformer of the NMR ensemble). **(c)** SWISS-MODEL (SM) [12] homology model of the EphA2-Sam (red)/Odin-Sam1 (blue) complex. The EphA2-Sam EH interface (residues I916-M918 and P952-Y960) is colored in yellow, violet and cyan, while the ML interface (residues L719-G742 in Odin-Sam1 **(a, c)** or residues H1219-G1240 of Ship2-Sam **(b)**) in light green, gold and orange, respectively in the Haddock model of the EphA2-Sam/Odin-Sam1 complex **(a)**, the NMR structure of EphA2-Sam bound to Ship2-Sam **(b)**, and in the homology model of EphA2-Sam/Odin-Sam1 complex **(c)**.

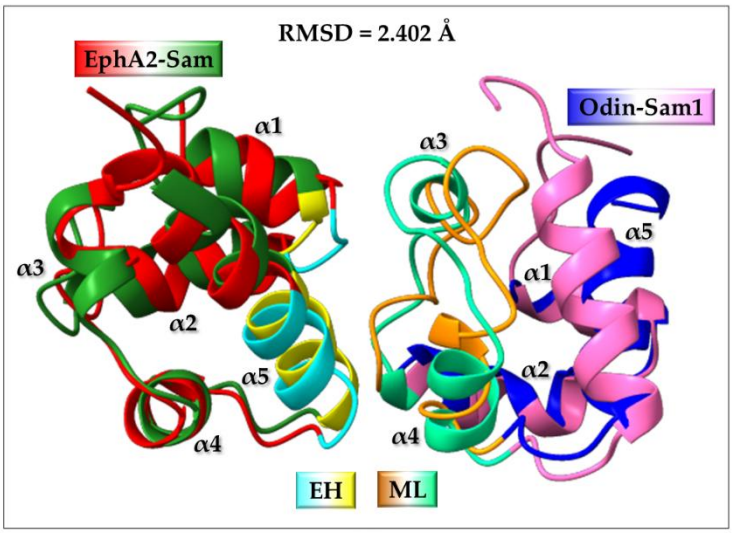

(a)

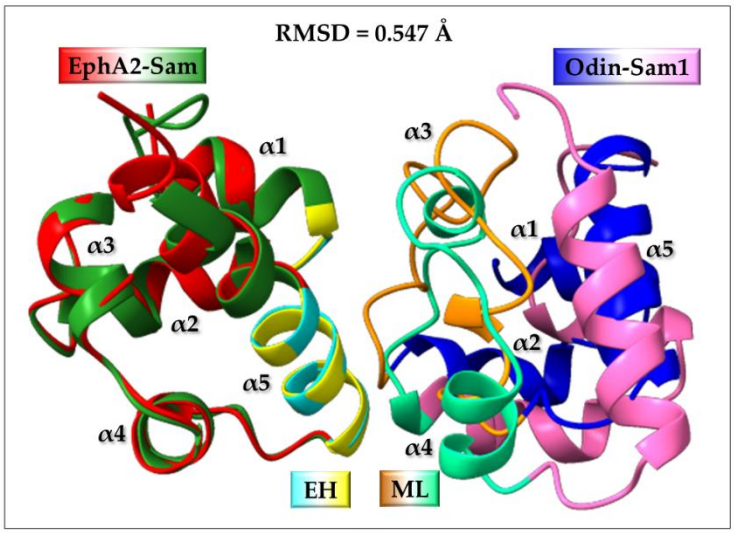

(b)

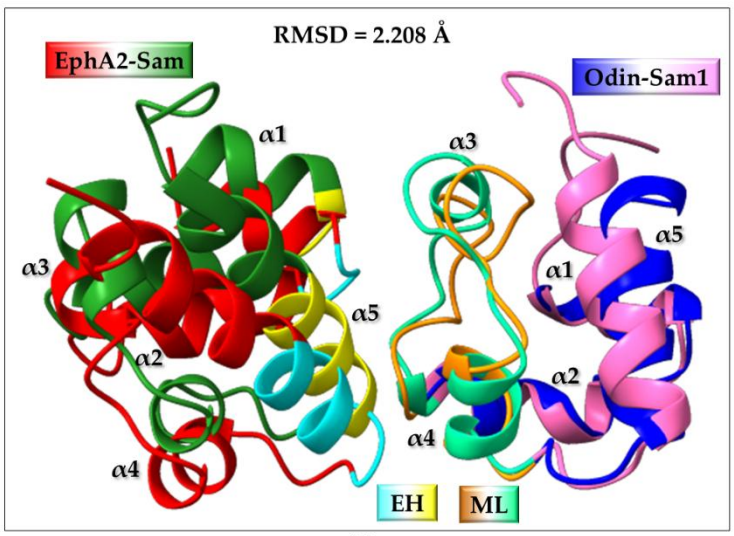

(c)

Figure S12. Overlays generated with Chimera X (v. 1.12) [13] between the Haddock model of the human EphA2-Sam (residues V904-Q968)/Odin-Sam1 (residue T696-V762) complex [5] and the SWISS-MODEL [12] predicted structure for human EphA2-Sam (residues T908-V972) in complex with Odin-Sam1 (residue S700-L759) [5]. EphA2-Sam and its EH region (residues I916-M918 and P952-Y960) are colored in forest green and yellow, respectively, in the docking pose, whereas they are reported in red and cyan, respectively, in the SWISS-MODEL generated structure. Regarding Odin-Sam1

and its ML region (residues L719-G742), they are reported in pink and light green and blue and orange, in the docking pose and in the SWISS-MODEL [12] structure, respectively. The structures have been overlayed on the backbone atoms (i.e., N, Cα and C′) of **(a)** both EphA2-Sam (residues T908-Q968) and Odin-Sam1 (residues S700-L759), **(b)** only EphA2-Sam (residues T908-Q968) and **(c)** only Odin-Sam1 (residues S700-L759); the corresponding RMSD values in Å, calculated with MolMol [14], are indicated in each panel.

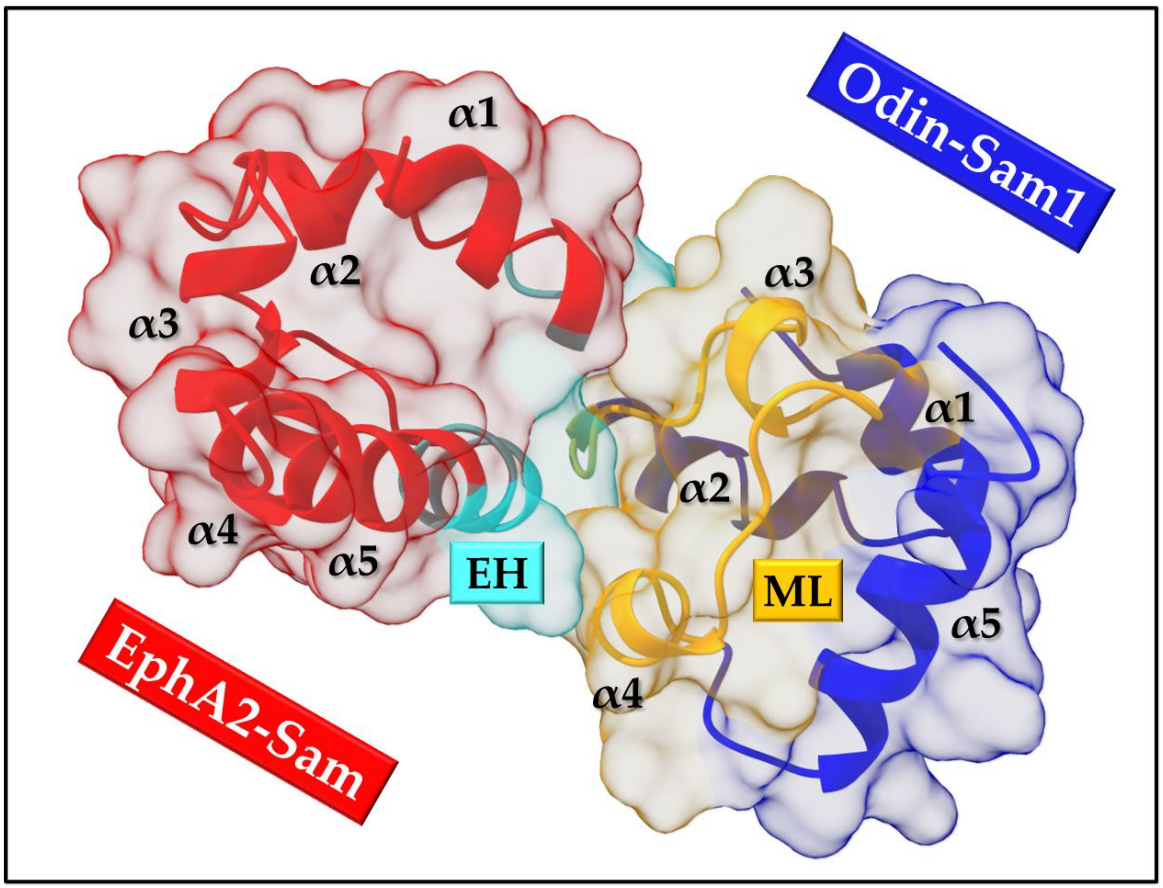

Figure S13. Validation of the in silico protocol. The best output structure from the Haddock Refinement Interface [15] for the Homo sapiens EphA2-Sam (UniProtKB [16] entry P29317 residues T908-V972) in complex with Homo sapiens Odin-Sam1 (UniProtKB [16] entry Q92625 residues S700-P760). The structure is reported in the ribbon drawing mode with a transparent surface; EphA2-Sam is colored red with the EH interface (EphA2-Sam residues I916-M918 and P952-Y960) colored cyan, whereas Odin-Sam1 is in blue with the ML (Odin-Sam1 residues L719-G742) interface in orange.

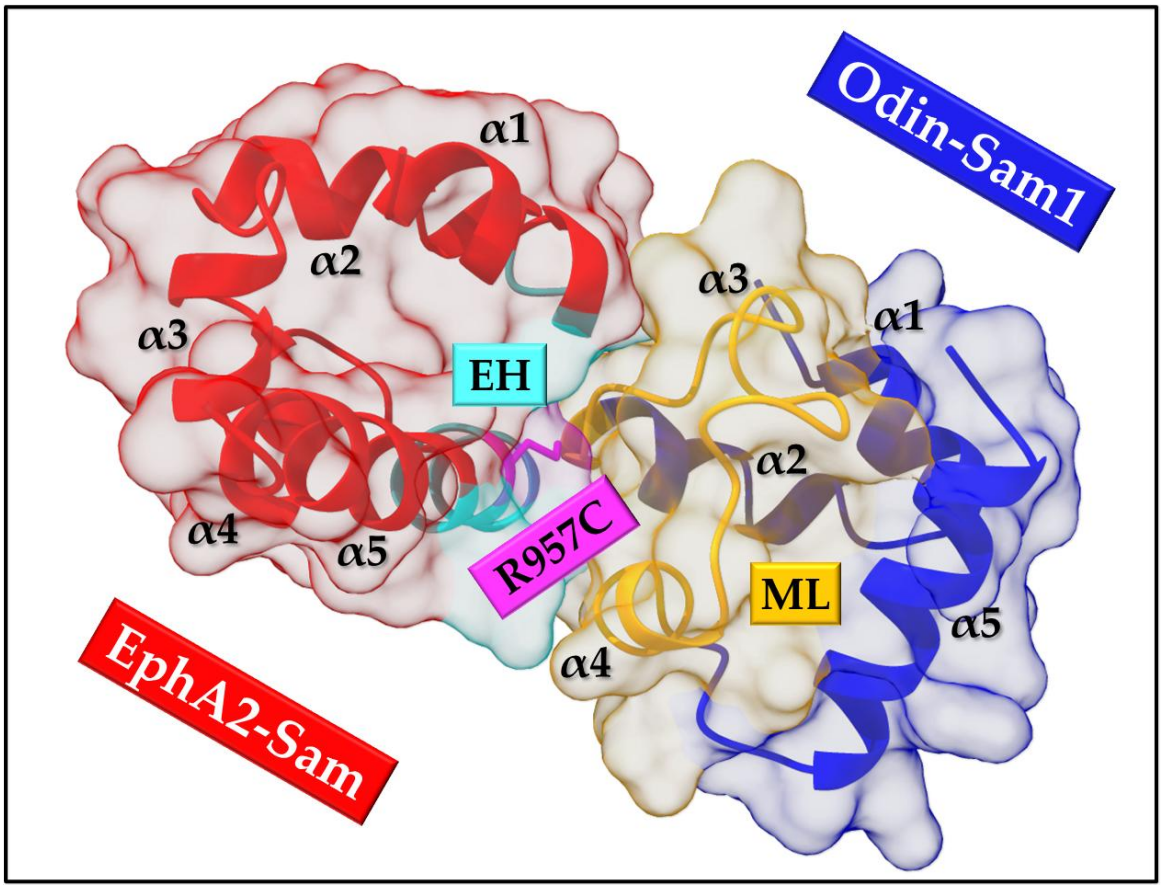

Figure S14. Validation of the in silico protocol. Ribbon representation of the best Haddock [15] structure for the Homo sapiens R957C EphA2-Sam variant (UniProtKB [16] entry P29317 residues T908-V972) in complex with Homo sapiens Odin-Sam1 (UniProtKB [16] entry Q92625 residues S700-P760). The EH and ML interaction interfaces in EphA2-Sam and Odin-Sam1 are colored in cyan and orange, respectively.

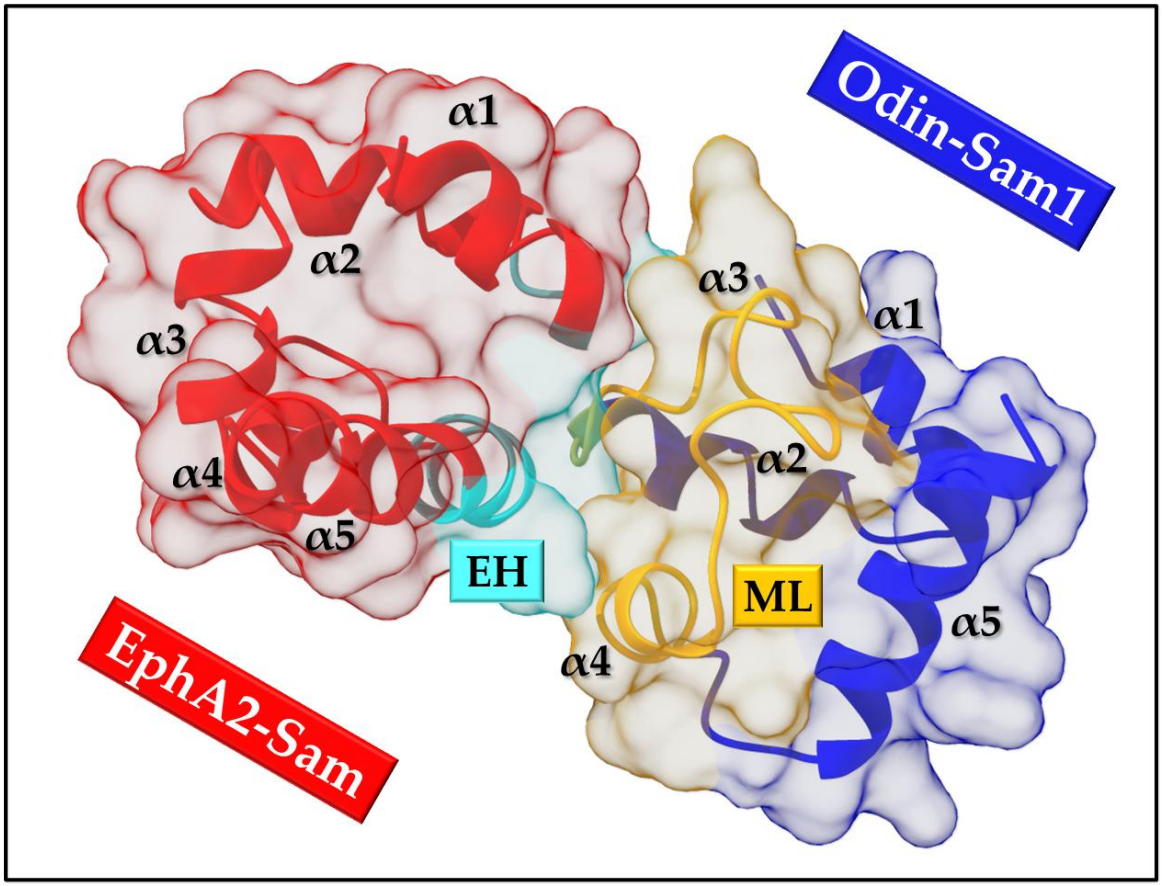

Figure S15. Validation of the in silico protocol. The best Haddock [15] structure for the Mus musculus EphA2-Sam (UniProtKB [16] entry Q03145 residues T909-V973) in complex with Mus musculus Odin-Sam1 (UniProtKB [16] entry P59672 residues S716-L775). The structure is shown in the ribbon drawing mode with a transparent surface. The EH and ML interaction interfaces in EphA2-Sam (residues I917-M919 and P953-Y961) and Odin-Sam1 (residues L735-G758) are presented in cyan and orange, respectively.

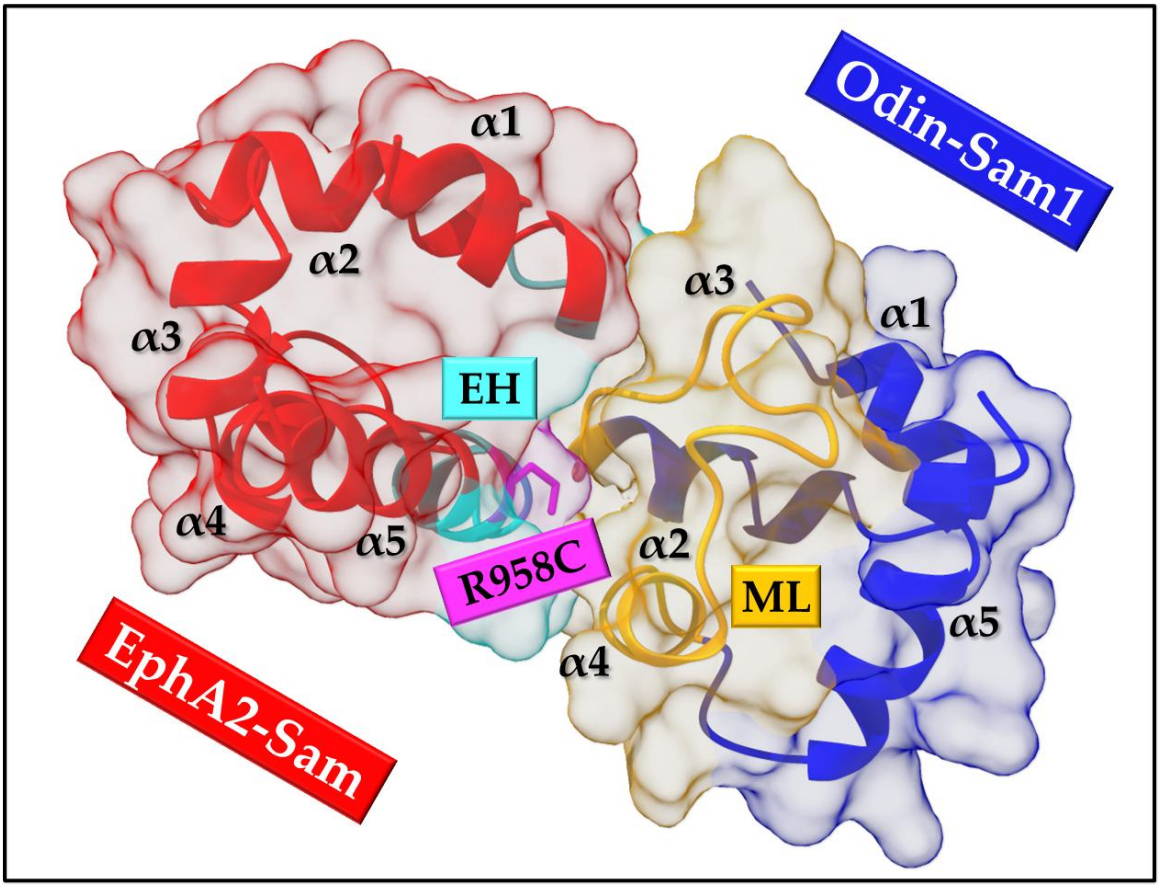

Figure S16. Validation of the in silico protocol. Ribbon representation of the best Haddock [15] structure for the Mus musculus R958C EphA2-Sam (UniProtKB [16] entry Q03145 residues T909-V973) variant in complex with Mus musculus Odin-Sam1 (UniProtKB [16] entry P59672 residues S716-L775). The EH and ML interaction interfaces in the R958C EphA2-Sam and Odin-Sam1 are colored in cyan and orange, respectively.

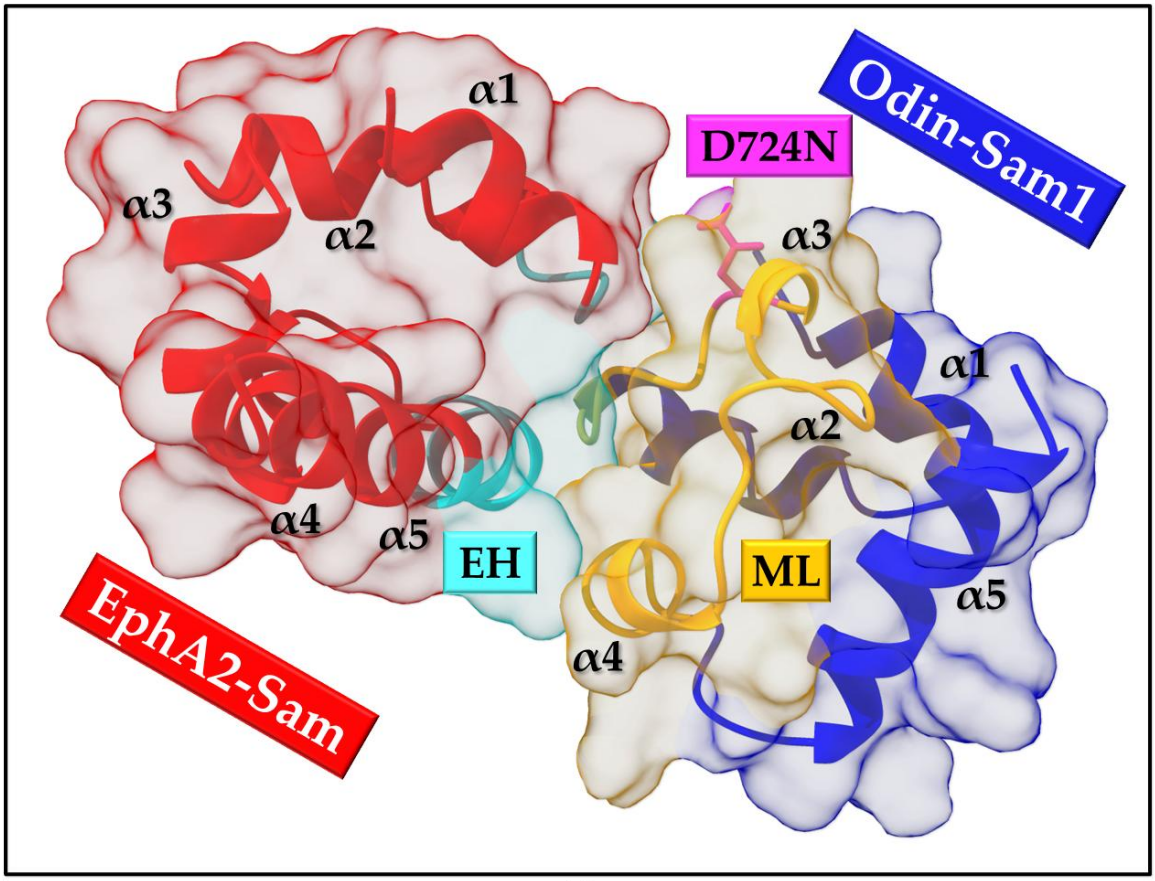

(a)

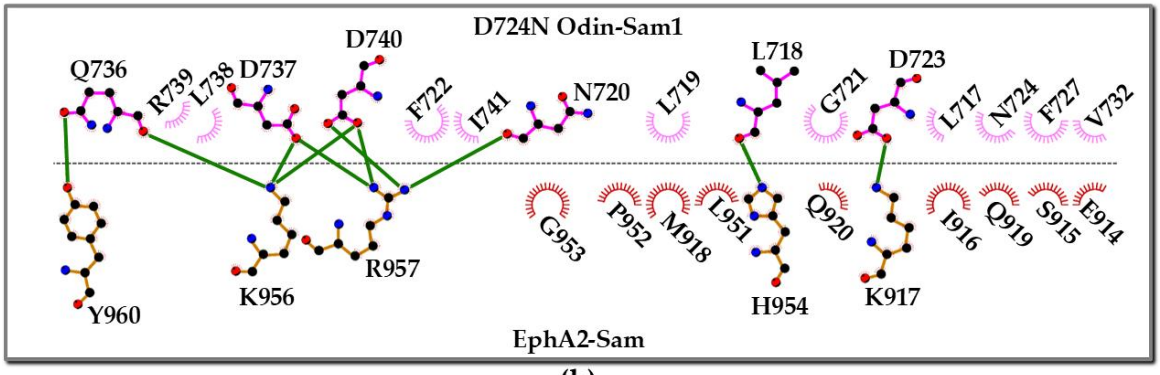

(b)

Figure S17. Results from the Haddock Refinement Interface run starting from the SM structure of EphA2-Sam in complex with Odin-Sam1. (**a**) Mixed ribbon/transparent surface representation of the best Haddock [15] structure for the EphA2-Sam/D724N Odin-Sam1 complex, the EH and ML interaction interfaces in EphA2-Sam and D724N Odin-Sam1 are colored in cyan and orange, respectively. The D724 mutated residue is colored magenta and its side-chain is shown in a neon representation. (**b**) 2D diagram of intermolecular interactions generated with LigPlot+ [17, 18] for the EphA2-Sam/D724N Odin-Sam1 complex shown in (**a**). Carbon, Nitrogen, and Oxygen atoms are indicated by black, blue, and red spheres, respectively. Maximum cutoffs for distances of H-acceptors of 2.7 Å and of donor-acceptor of 3.35 Å were set to find H-bonds (= green solid lines). EphA2-Sam and D724N Odin-Sam1 residues involved in further non-bonded interactions are labeled with the one-letter amino acid code and residue number and represented by red and pink crescents with bristles, respectively.

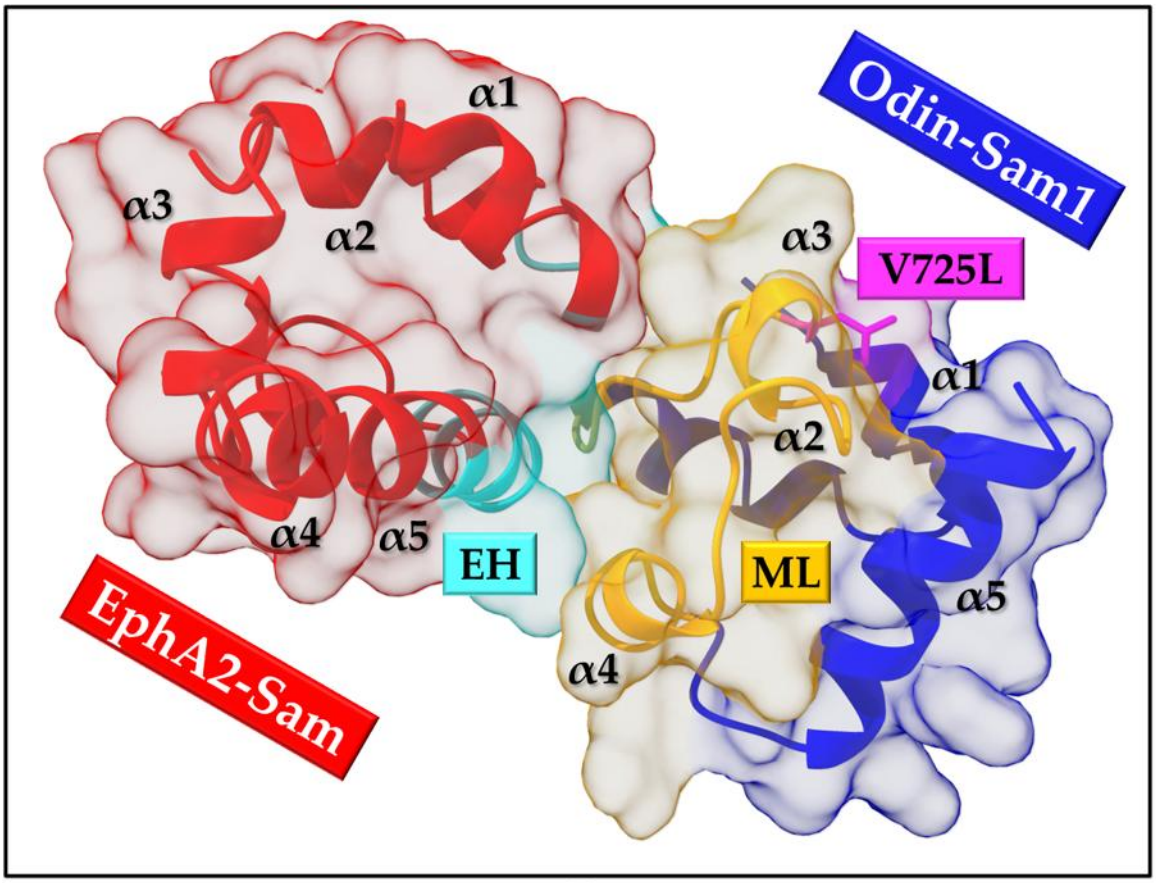

(a)

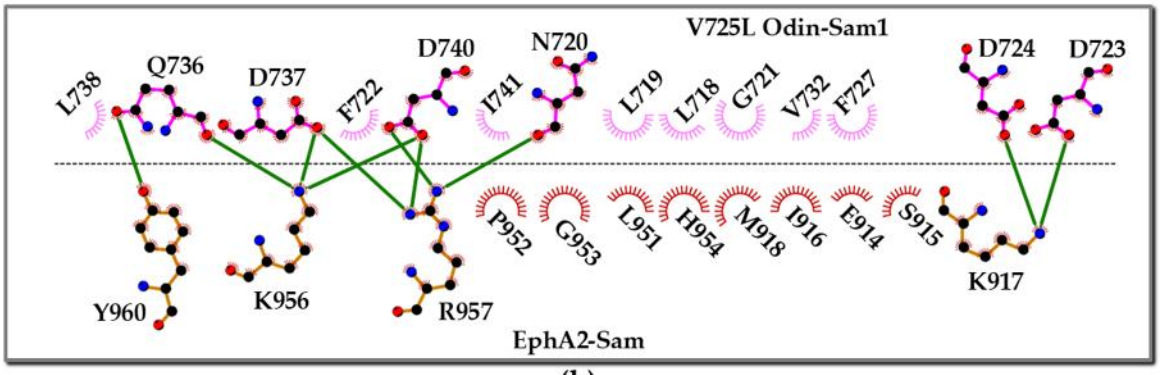

(b)

Figure S18. Results from the Haddock Refinement Interface run starting from the SM structure of EphA2-Sam in complex with Odin-Sam1. (**a**) Mixed ribbon/transparent surface representation of the best Haddock [15] structure for the EphA2-Sam/V725L Odin-Sam1 complex, the EH and ML interaction interfaces in EphA2-Sam and V725L Odin-Sam1 are colored in cyan and orange, respectively. The mutated residue (L725) is colored magenta and its side-chain is shown in a neon representation. (**b**) 2D diagram of intermolecular interactions generated with LigPlot+ [17, 18] for the EphA2-Sam/V725L Odin-Sam1 complex shown in (**a**). The solid green lines and the crescents with bristles represent H-bonds and non-bonded contacts, respectively.

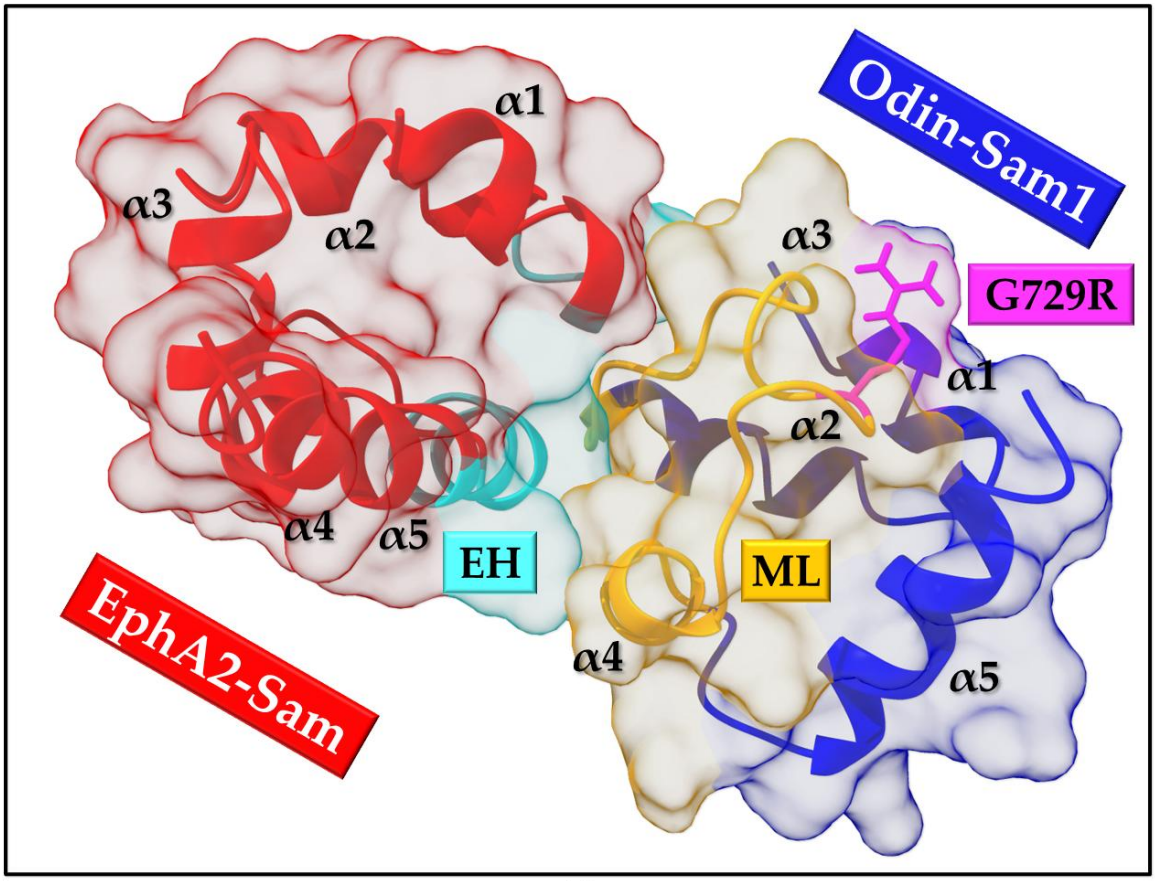

(a)

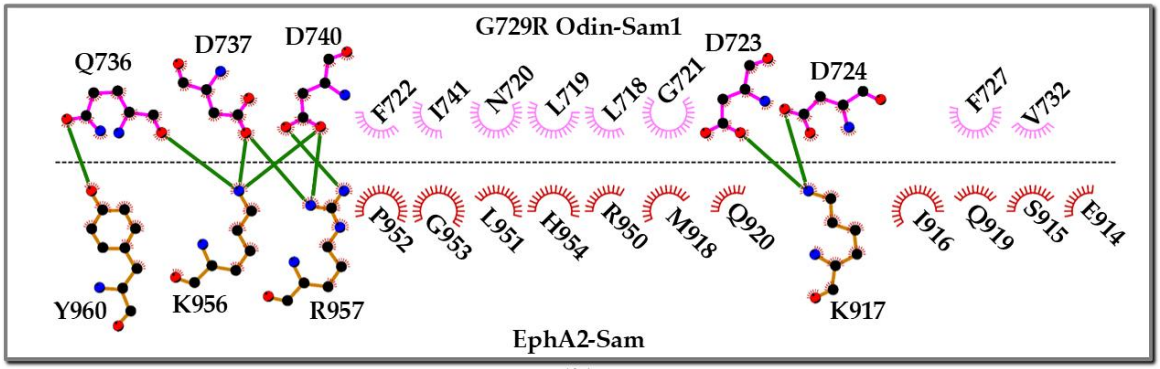

(b)

Figure S19. Results from the Haddock Refinement Interface run starting from the SM structure of EphA2-Sam in complex with Odin-Sam1. (**a**) Mixed ribbon/transparent surface representation of the best Haddock [15] structure for the EphA2-Sam/G729R Odin-Sam1 complex, the EH and ML interaction interfaces in EphA2-Sam and G729R Odin-Sam1 are colored in cyan and orange, respectively. The mutated residue (R729) is colored magenta and its side-chain is shown in a neon representation. (**b**) 2D diagram of intermolecular interactions generated with LigPlot+ [17, 18] for the EphA2-Sam/G729R Odin-Sam1 complex shown in (**a**). The solid green lines and the crescents with bristles represent H-bonds and non-bonded contacts, respectively.

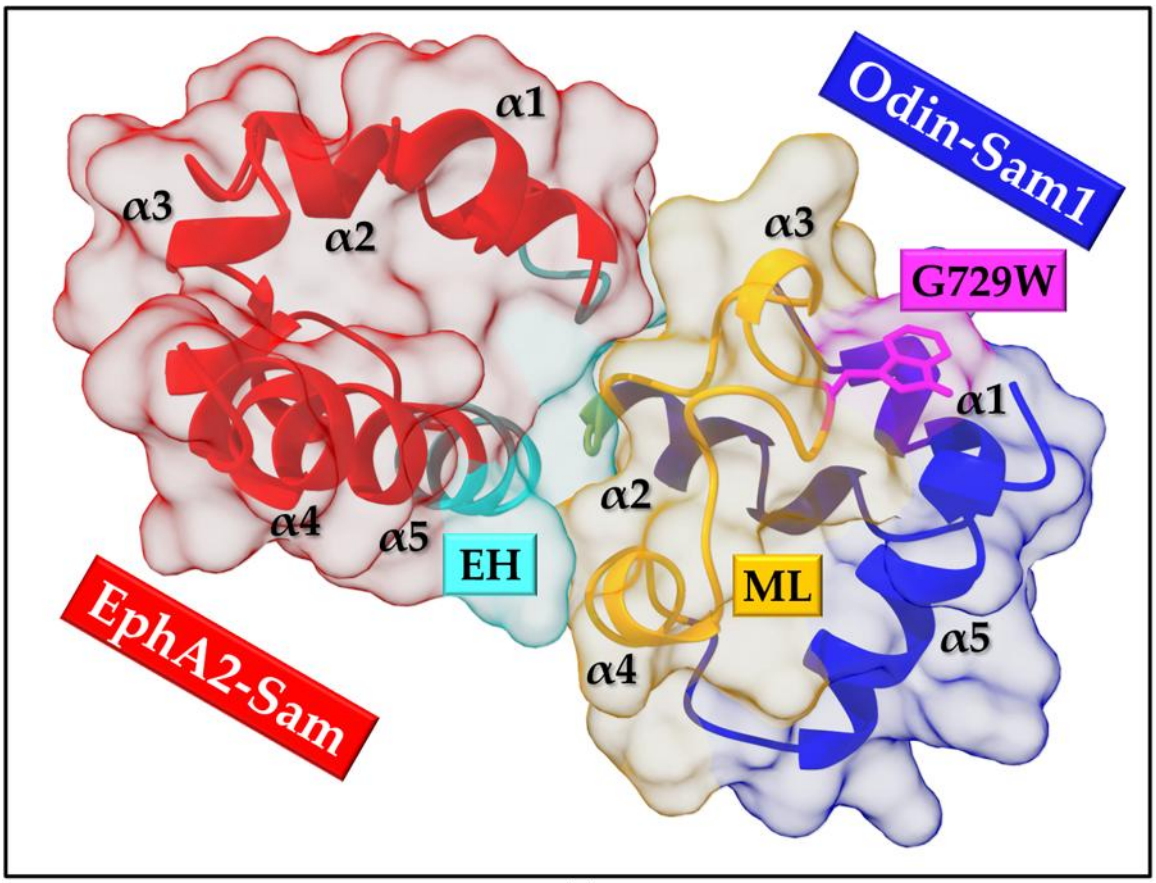

(a)

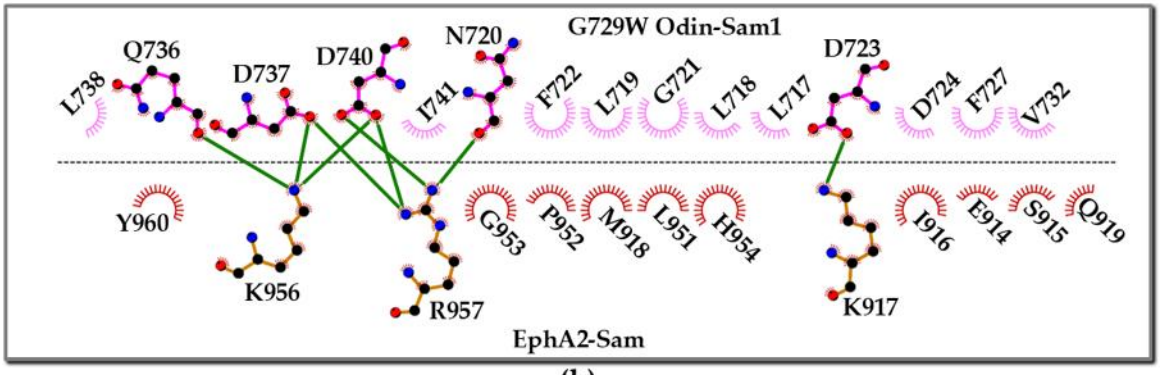

(b)

Figure S20. Results from the Haddock Refinement Interface run starting from the SM structure of EphA2-Sam in complex with Odin-Sam1. (**a**) Mixed ribbon/transparent surface representation of the best Haddock [15] structure for the EphA2-Sam/G729W Odin-Sam1 complex, the EH and ML interaction interfaces in EphA2-Sam and G729W Odin-Sam1 are colored in cyan and orange, respectively. The mutated residue (W729) is colored magenta and its side-chain is shown in a neon representation. (**b**) 2D diagram of intermolecular interactions generated with LigPlot+ [17, 18] for the EphA2-Sam/G729W Odin-Sam1 complex shown in (**a**). The solid green lines and the crescents with bristles represent H-bonds and non-bonded contacts, respectively.

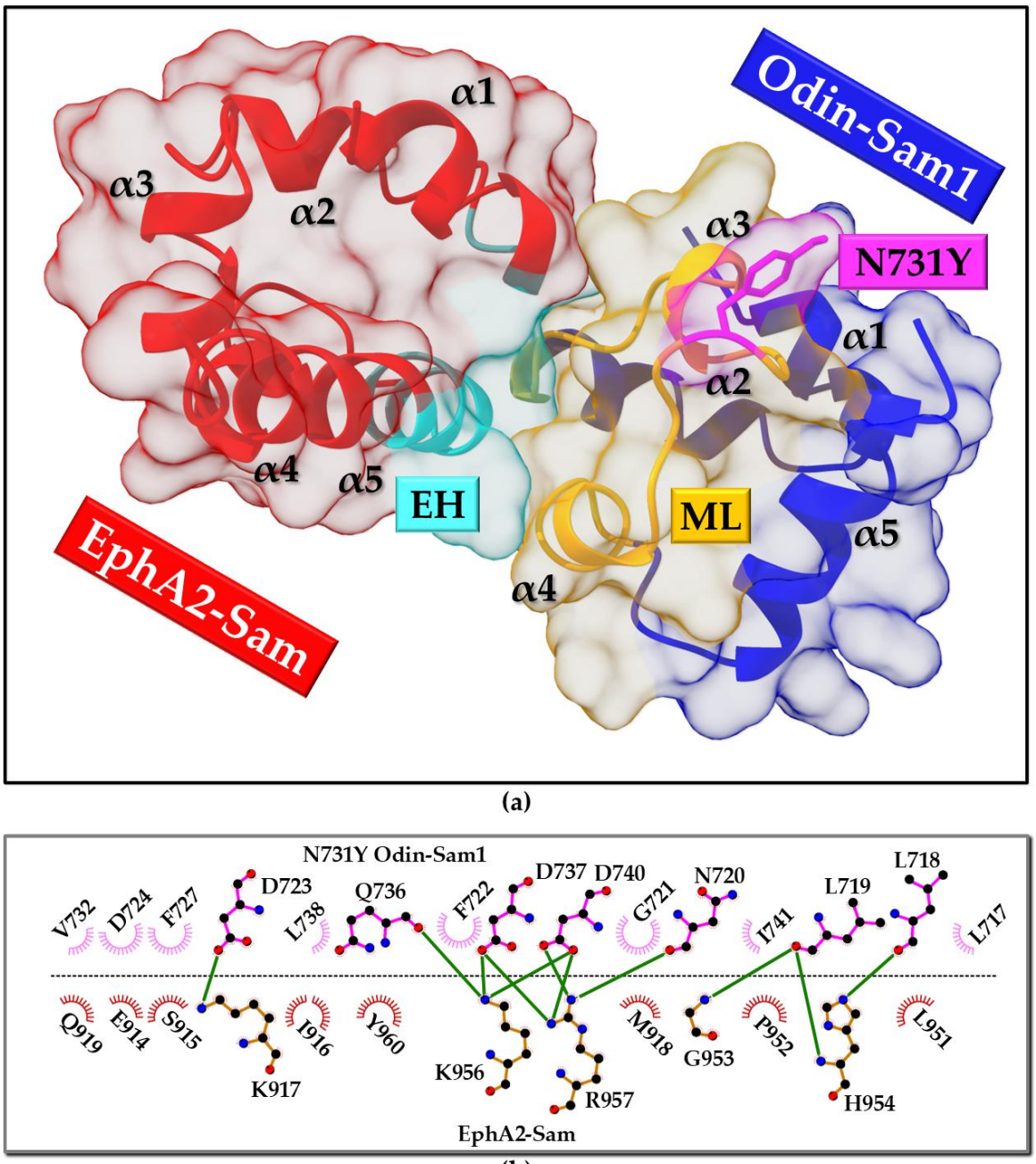

Figure S21. Results from the Haddock Refinement Interface run starting from the SM structure of EphA2-Sam in complex with Odin-Sam1. (**a**) Mixed ribbon/transparent surface representation of the best Haddock [15] structure for the EphA2-Sam/N731Y Odin-Sam1 complex, the EH and ML interaction interfaces in EphA2-Sam and N731Y Odin-Sam1 are colored in cyan and orange, respectively. The mutated residue (Y731) is colored magenta and its side-chain is shown in a neon representation. (**b**) 2D diagram of intermolecular interactions generated with LigPlot+ [17, 18] for the EphA2-Sam/N731Y Odin-Sam1 complex shown in (**a**). The solid green lines and the crescents with bristles represent H-bonds and non-bonded contacts, respectively.

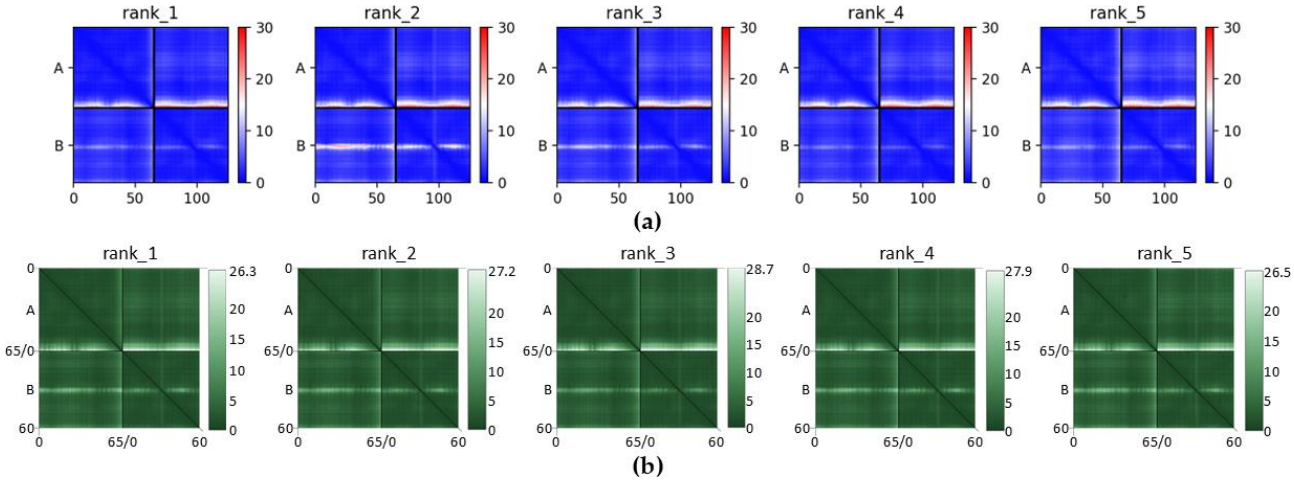

Figure S22. PAE (Predicted Aligned Error) plots of the five AF2 [8, 9] **(a)** and AF3 [10] **(b)** models of the wild-type EphA2-Sam (chain A)/Odin-Sam1 (chain B) complex. Each plot is flanked by a PAE score scale, where the values range from < 5 Å (dark blue for AF2 plots and dark green for AF3 plots), related to very low PAE and high confidence, to > 20 Å (dark red for AF2 plots and white for AF3 plots), related to high PAE and low confidence in the relative position of X and Y residues. In all plots, the top-left and bottom-right squared regions represent intra-chain scores [19, 20].

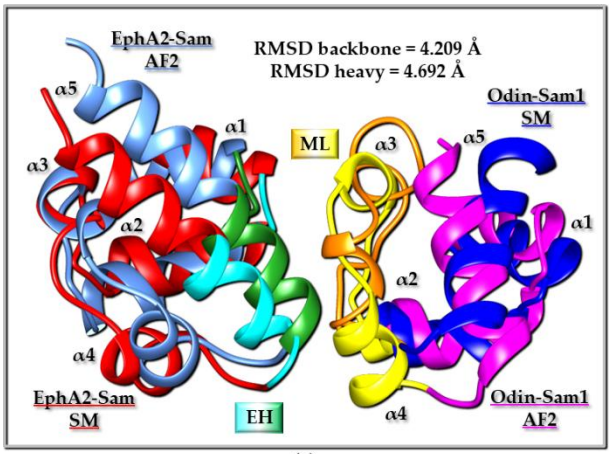

(a)

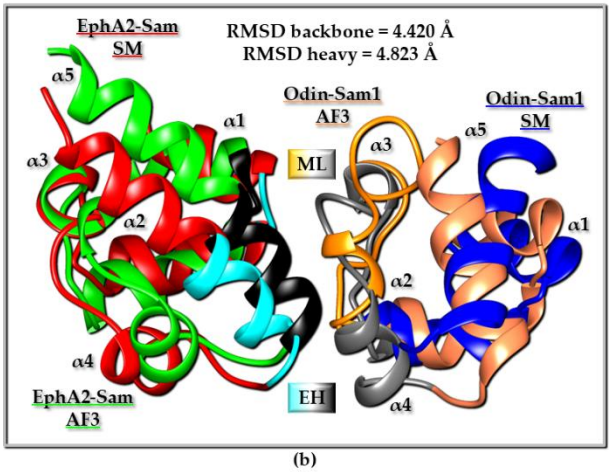

(b)

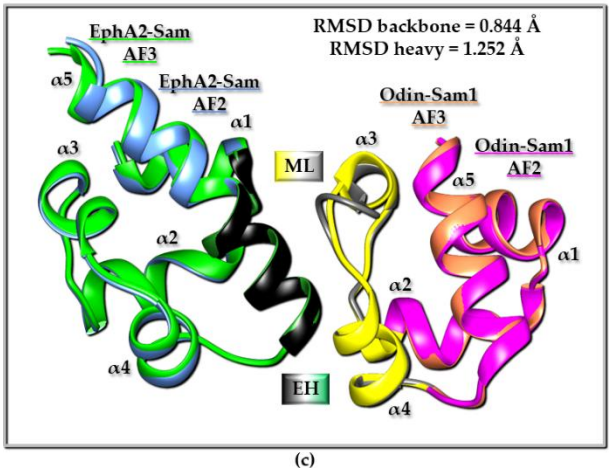

(c)

Figure S23. Overlays generated with UCSF Chimera (v. 1.20) [7] between the SM [12], best AF2 [8, 9], and AF3 [10] predicted structures of human EphA2-Sam (residues T908-V972) in complex with Odin-Sam1 (residues S700-L759). EphA2-Sam is colored in red, cornflower blue, and light green, respectively, in the SM [12], AF2 [8] and AF3 [10] structures. The EH region (residues I916-M918 and P952-Y960) of EphA2-Sam is shown in cyan, dark green, and black, respectively, in the SM [12], AF2 [8, 9], and AF3 [10] structures. Odin-Sam1 is colored in blue, magenta, and coral, respectively, in the SM [12], AF2 [8, 9], and AF3 [10] structures. The ML region (residues L719-G742) of Odin-Sam1 is shown in orange, yellow, and dark grey in the SM [12], AF2 [8, 9] and AF3 [10] structures. The structures have been overlayed on the backbone atoms (i.e., N, Cα and C') of both EphA2-Sam (residues T908-V972) and Odin-Sam1 (residues S700-L759) for **(a)** SM [12] and AF2 [8, 9] predicted structures, **(b)** SM [12] and AF3 [10] predicted structures, and **(c)** AF2 [8, 9] and AF3 [10] predicted structures. The corresponding RMSD values in Å, calculated with MolMol [14], are indicated in each panel. RMSD values over the heavy atoms (i.e., C, N, O, S) are also reported for each panel. Regarding AF structures only the best among the five computed models were considered.

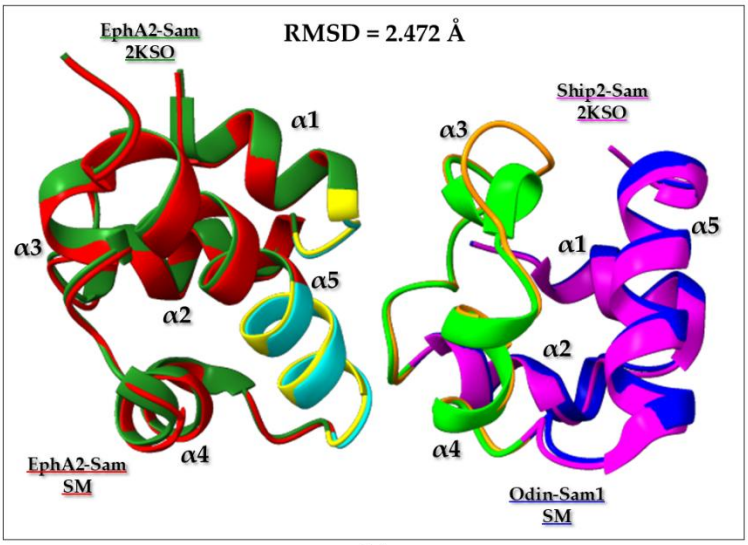

(a)

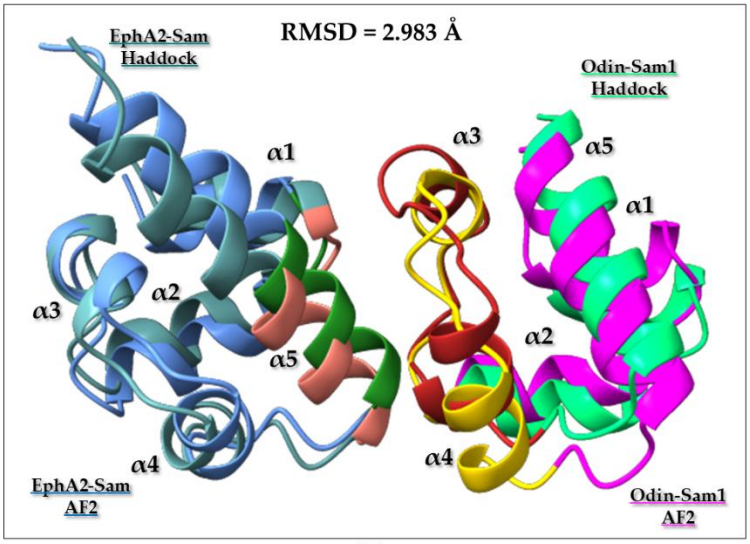

(b)

Figure S24. Overlays on the backbone atoms generated with Chimera X (v. 1.12) [13], between **(a)** the NMR solution structure of the human EphA2-Sam (forest green)/Ship2-Sam (violet) complex (pdb id 2KSO [11], first conformer of the NMR ensemble) and the SM [12] predicted structure for human EphA2-Sam (residues T908-V972-red) in complex with Odin-Sam1 (residue S700-L759-blue), and **(b)** the Haddock [15] model of the human EphA2-Sam (residues T908-V972 dark cyan)/Odin-Sam1 (residue S700-L759 light green) complex [5] and the AF2 [8, 9] predicted structure of the human EphA2-Sam (residues T908-V972-light blue)/Odin-Sam1 (residue S700-L759-magenta) complex. EphA2-Sam EH region (residues I916-M918 and P952-Y960) is colored in yellow, cyan, pink and forest green in 2KSO, SM, Haddock and AF2 models, respectively. The ML region (residues L719-G742 in Odin-Sam1; residues H1219-G1240 of Ship2-Sam) is colored green, orange, dark red and gold in 2KSO, SM, Haddock and AF2 models, respectively. The RMSD values in Å are indicated in the a and b panels.

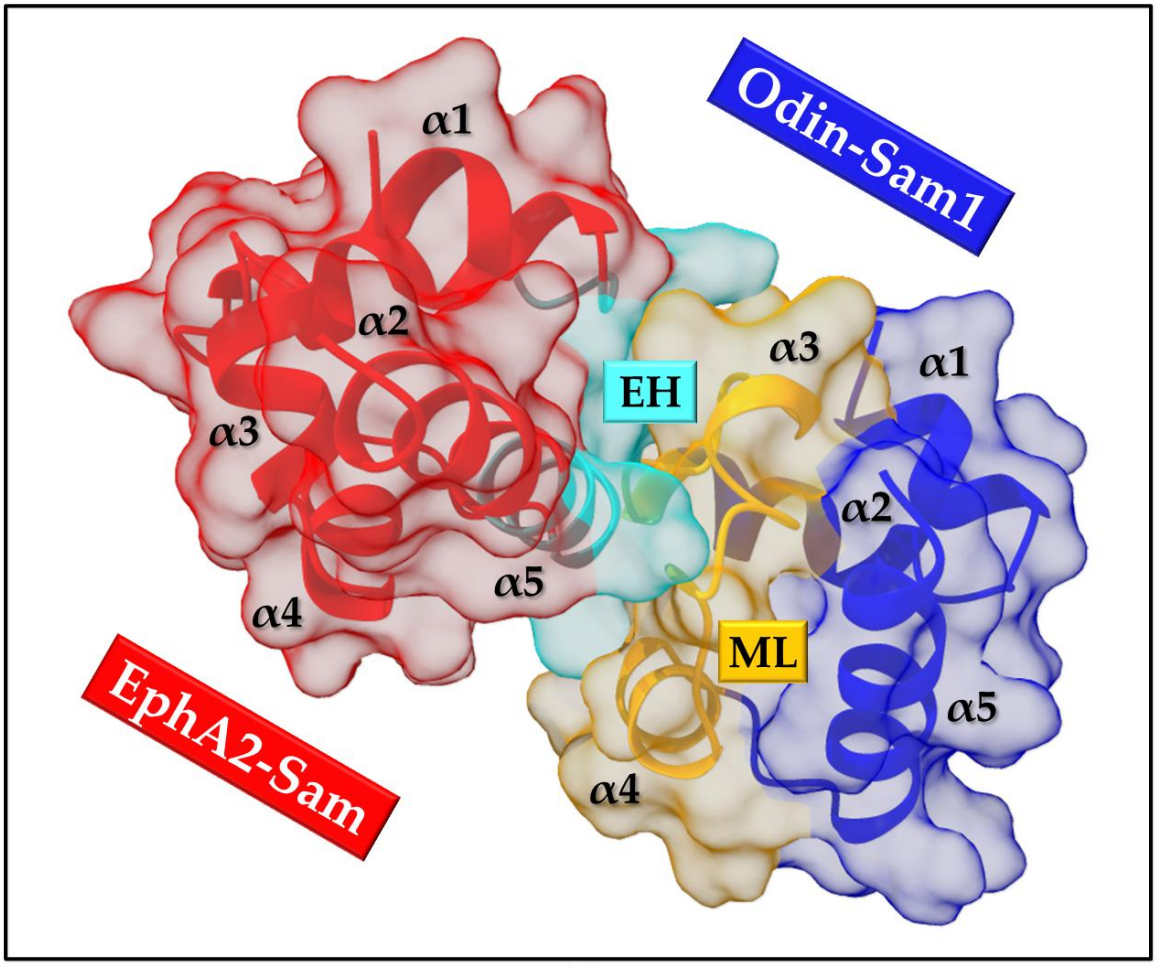

(a)

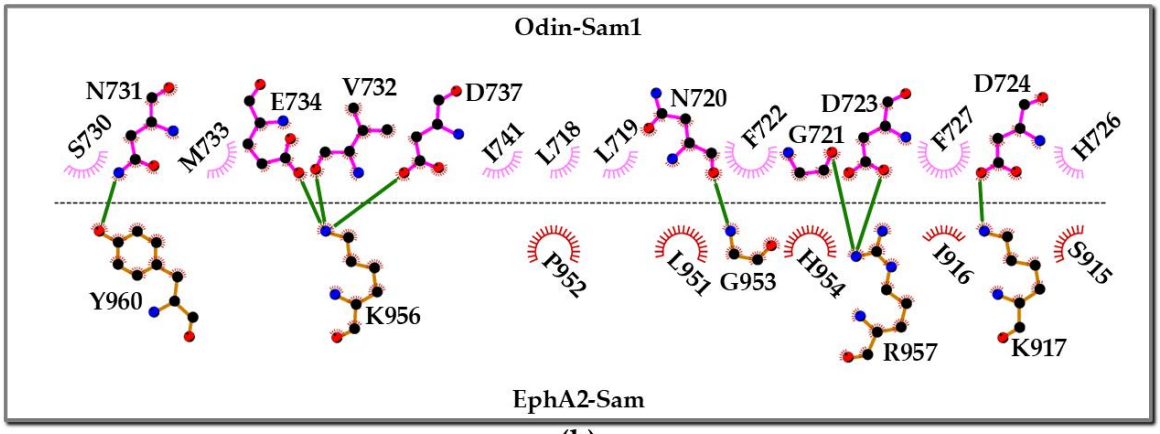

(b)

Figure S25. (a) Ribbon representation of the best Haddock [15] refined structure generated for the EphA2-Sam/Odin-Sam1 complex starting from its five AF2 [8, 9] models. The EH and ML interaction interfaces in EphA2-Sam and Odin-Sam1 are colored in cyan and orange, respectively. **(b)** 2D diagram of intermolecular interactions generated with LigPlot+ [17, 18] for the EphA2-Sam/Odin-Sam1 complex shown in **(a)**. The solid green lines and the crescents with bristles represent H-bonds and non-bonded contacts, respectively.

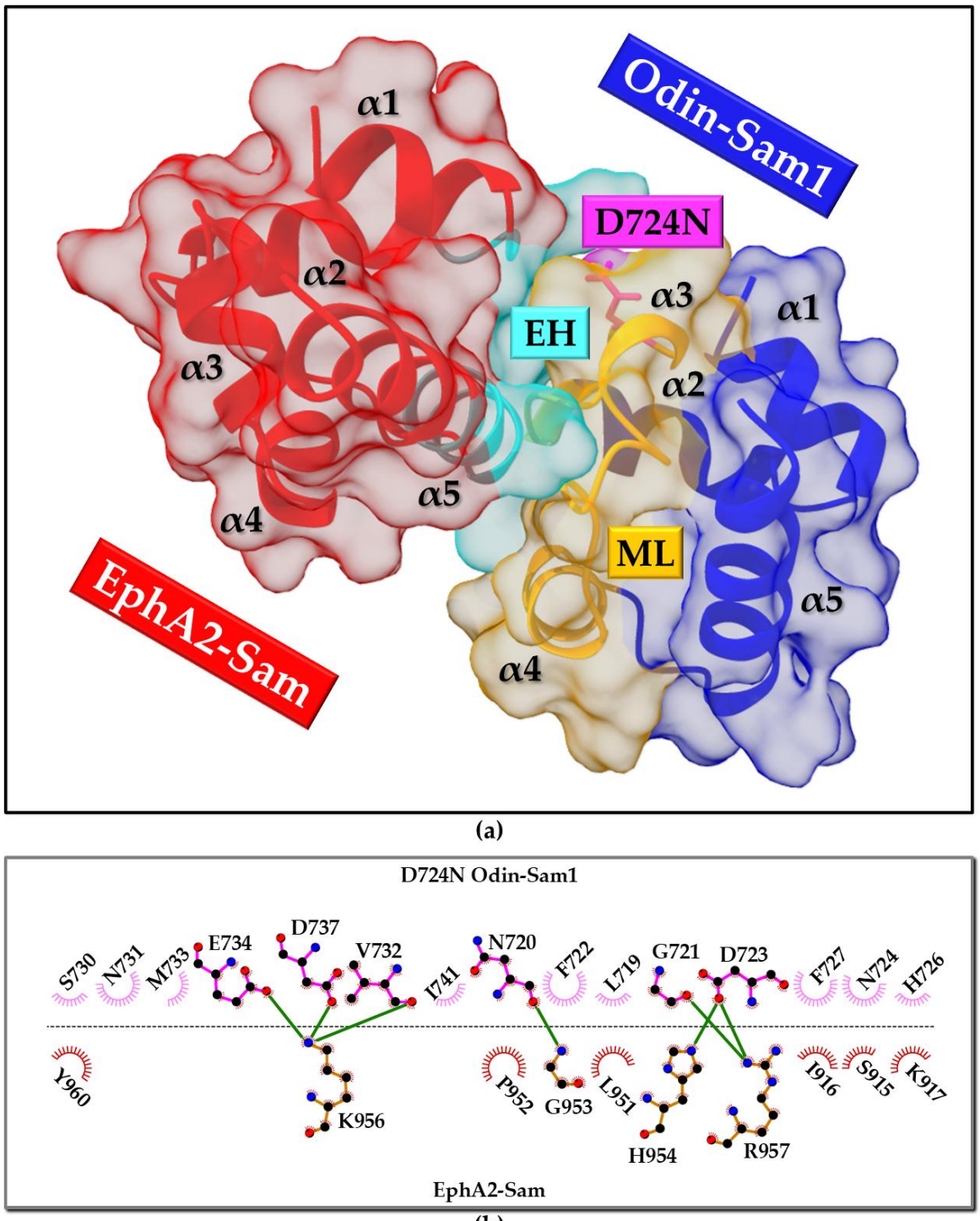

Figure S26. (a) Ribbon representation of the best Haddock [15] structure generated for the EphA2-Sam/D724N Odin-Sam1 complex starting from the five AF2 [8, 9] models of the native EphA2-Sam/Odin-Sam1 complex. The EH and ML interaction interfaces in EphA2-Sam and D724N Odin-Sam1 are colored in cyan and orange, respectively. **(b)** 2D diagram of intermolecular interactions generated with LigPlot+ [17, 18] for the EphA2-Sam/D724N Odin-Sam1 complex shown in **(a)**. The solid green lines and the crescents with bristles represent H-bonds and non-bonded contacts, respectively.

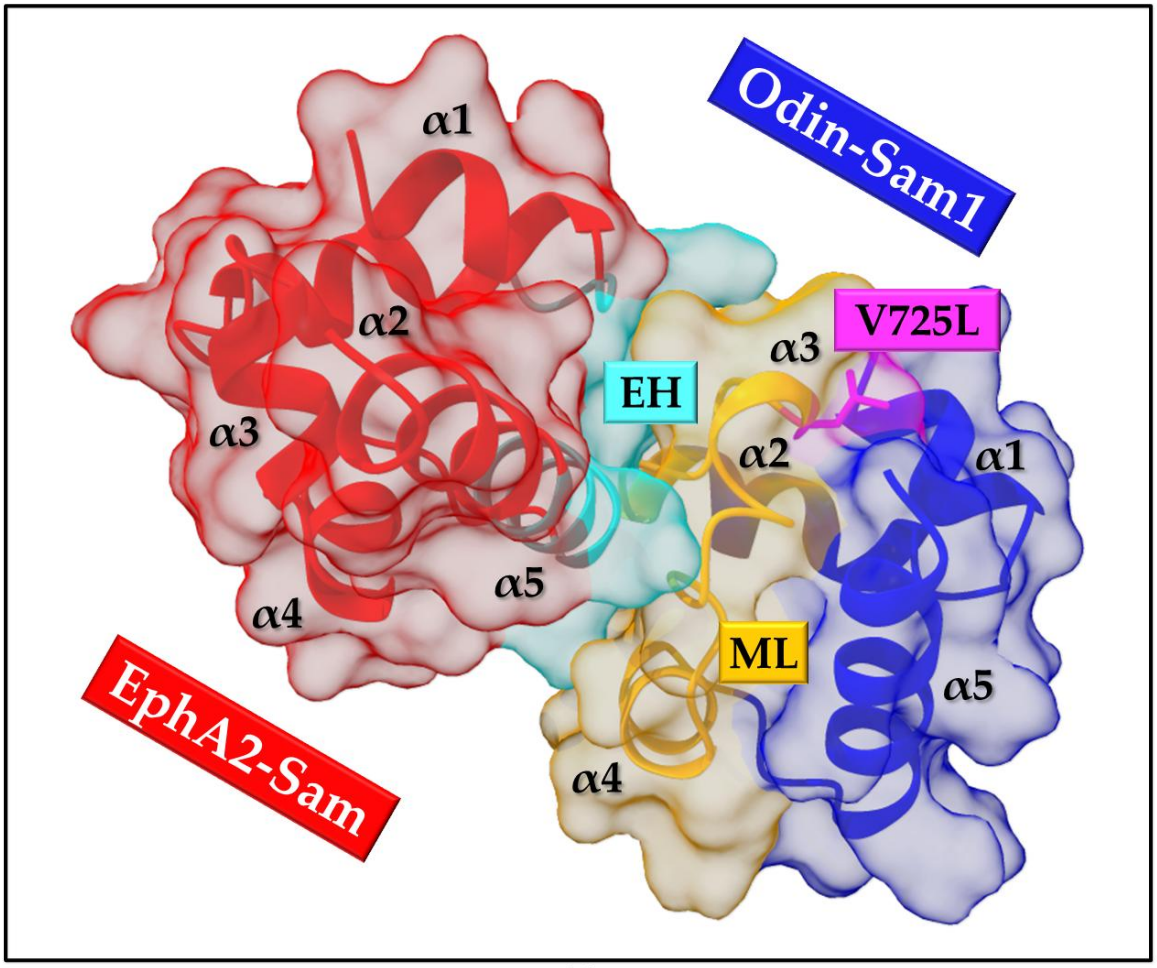

(a)

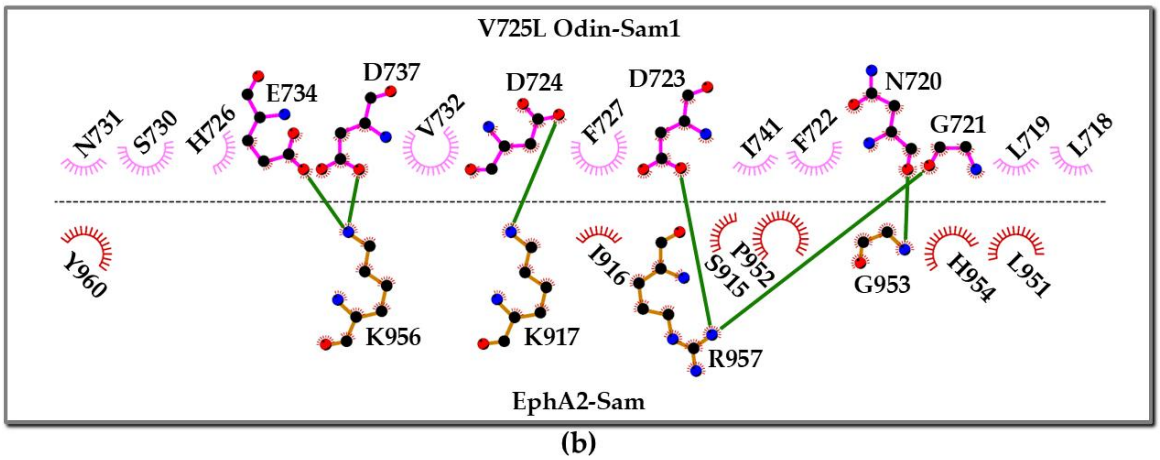

(b)

Figure S27. (a) Ribbon representation of the best Haddock [15] structure generated for the EphA2-Sam/V725L Odin-Sam1 complex employing the five AF2 [8, 9] models of the native EphA2-Sam/Odin-Sam1 complex as input. The EH and ML interaction interfaces in EphA2-Sam and V725L Odin-Sam1 are colored in cyan and orange, respectively. **(b)** 2D diagram of intermolecular interactions generated with LigPlot+ [17, 18] for the EphA2-Sam/V725L Odin-Sam1 complex shown in **(a)**. The solid green lines and the crescents with bristles represent H-bonds and non-bonded contacts, respectively.

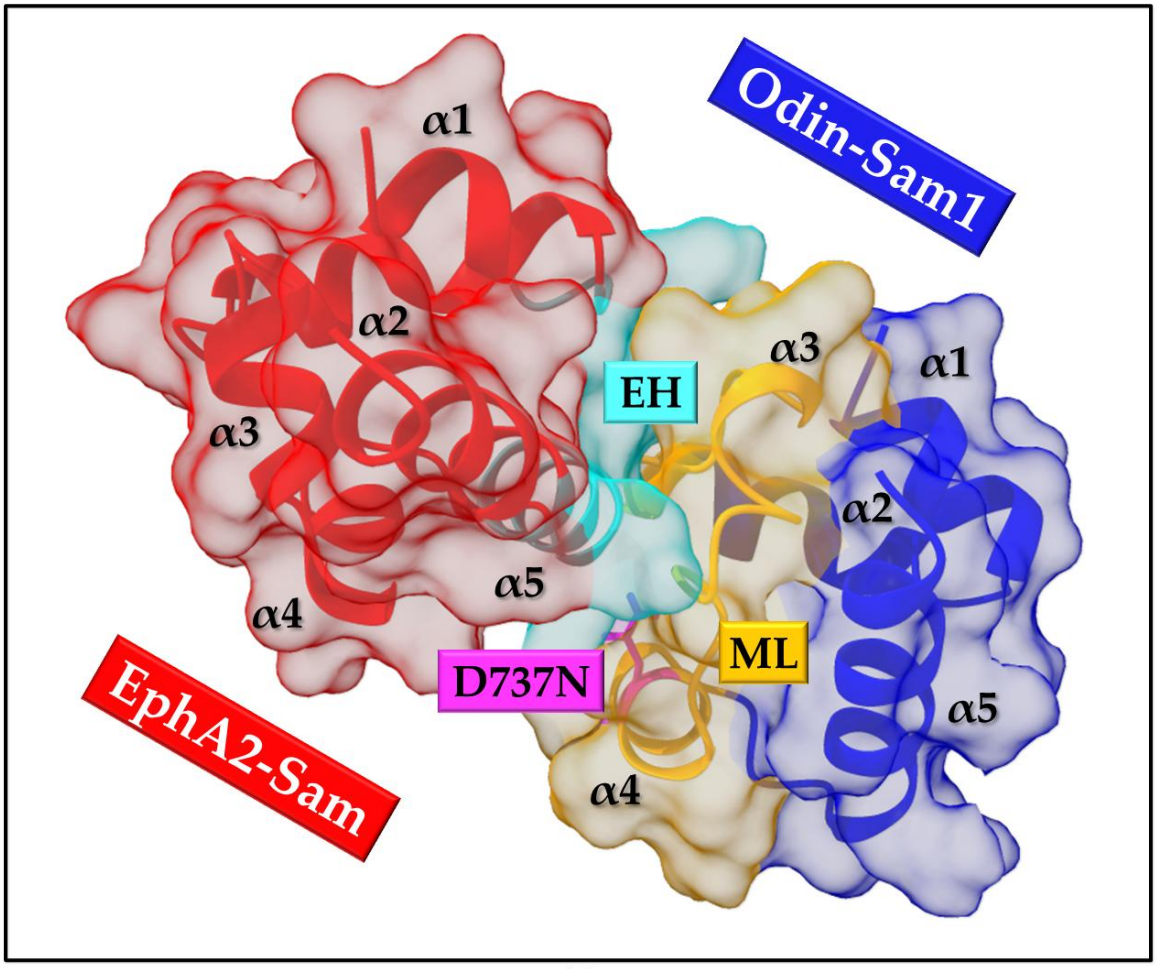

(a)

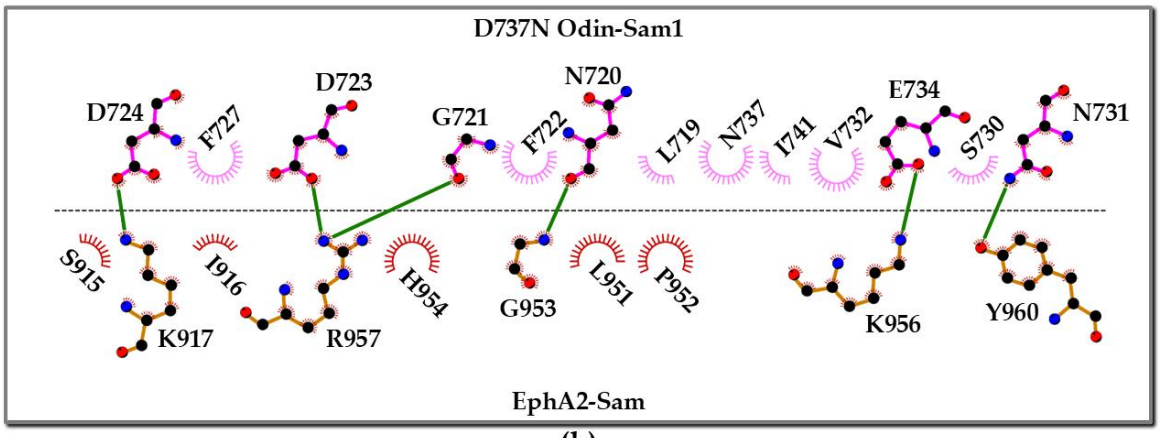

(b)

Figure S28. (a) Ribbon representation of the best Haddock [15] structure generated for the EphA2-Sam/D737N Odin-Sam1 complex starting from the five AF2 [8, 9] models of the native EphA2-Sam/Odin-Sam1 complex as input. The EH and ML interaction interfaces in EphA2-Sam and D737N Odin-Sam1 are colored in cyan and orange, respectively. **(b)** 2D diagram of intermolecular interactions generated with LigPlot+ [17, 18] for the EphA2-Sam/D737N Odin-Sam1 complex shown in **(a)**. The solid green lines and the crescents with bristles represent H-bonds and non-bonded contacts, respectively.

References

1. Huang, X.; Miller, W. A Time-Efficient, Linear-Space Local Similarity Algorithm. *Adv. Appl. Math.* **1991,** *12*, 337–357. Corresponding to reference 34 in the main text.
2. Wilkins, M. R.; Gasteiger, E.; Bairoch, A.; Sanchez, J. C.; Williams, K. L.; Appel, R. D.; Hochstrasser, D. F. Protein identification and analysis tools in the ExPASy server. *Methods Mol. Biol.* **1999,** *112*, 531–52. Corresponding to reference 62 in the main text.
3. Venselaar, H.; Te Beek, T. A.; Kuipers, R. K.; Hekkelman, M. L.; Vriend, G. Protein structure analysis of mutations causing inheritable diseases. An e-Science approach with life scientist friendly interfaces. *BMC Bioinformatics* **2010,** *11*, 548. Corresponding to reference 61 in the main text.
4. Vander Meersche, Y.; Cretin, G.; de Brevern, A. G.; Gelly, J. C.; Galochkina, T. MEDUSA: Prediction of Protein Flexibility from Sequence. *J. Mol. Biol.* **2021,** *433*, 166882. Corresponding to reference 66 in the main text.
5. Mercurio, F. A.; Marasco, D.; Pirone, L.; Pedone, E. M.; Pellecchia, M.; Leone, M. Solution structure of the first Sam domain of Odin and binding studies with the EphA2 receptor. *Biochemistry* **2012,** *51*, 2136–45. Corresponding to reference 12 in the main text.
6. Schymkowitz, J.; Borg, J.; Stricher, F.; Nys, R.; Rousseau, F.; Serrano, L. The FoldX web server: an online force field. *Nucleic Acids Res.* **2005,** *33*, W382–8. Corresponding to reference 57 in the main text.
7. Pettersen, E. F.; Goddard, T. D.; Huang, C. C.; Couch, G. S.; Greenblatt, D. M.; Meng, E. C.; Ferrin, T. E. UCSF Chimera--a visualization system for exploratory research and analysis. *J. Comput. Chem.* **2004,** *25*, 1605–12. Corresponding to reference 58 in the main text.
8. Jumper, J.; Evans, R.; Pritzel, A.; Green, T.; Figurnov, M.; Ronneberger, O.; Tunyasuvunakool, K.; Bates, R.; Zidek, A.; Potapenko, A.; Bridgland, A.; Meyer, C.; Kohl, S. A. A.; Ballard, A. J.; Cowie, A.; Romera-Paredes, B.; Nikolov, S.; Jain, R.; Adler, J.; Back, T.; Petersen, S.; Reiman, D.; Clancy, E.; Zielinski, M.; Steinegger, M.; Pacholska, M.; Berghammer, T.; Bodenstein, S.; Silver, D.; Vinyals, O.; Senior, A. W.; Kavukcuoglu, K.; Kohli, P.; Hassabis, D. Highly accurate protein structure prediction with AlphaFold. *Nature* **2021,** *596*, 583–589. Corresponding to reference 29 in the main text.
9. Bertoline, L. M. F.; Lima, A. N.; Krieger, J. E.; Teixeira, S. K. Before and after AlphaFold2: An overview of protein structure prediction. *Front. Bioinform.* **2023,** *3*, 1120370. Corresponding to reference 28 in the main text.
10. Abramson, J.; Adler, J.; Dunger, J.; Evans, R.; Green, T.; Pritzel, A.; Ronneberger, O.; Willmore, L.; Ballard, A. J.; Bambrick, J.; Bodenstein, S. W.; Evans, D. A.; Hung, C. C.; O'Neill, M.; Reiman, D.; Tunyasuvunakool, K.; Wu, Z.; Zemgulyte, A.; Arvaniti, E.; Beattie, C.; Bertolli, O.; Bridgland, A.; Cherepanov, A.; Congreve, M.; Cowen-Rivers, A. I.; Cowie, A.; Figurnov, M.; Fuchs, F. B.; Gladman, H.; Jain, R.; Khan, Y. A.; Low, C. M. R.; Perlin, K.; Potapenko, A.; Savy, P.; Singh, S.; Stecula, A.; Thillaisundaram, A.; Tong, C.; Yakneen, S.; Zhong, E. D.; Zielinski, M.; Zidek, A.; Bapst, V.; Kohli, P.; Jaderberg, M.; Hassabis, D.; Jumper, J. M. Accurate structure prediction of biomolecular interactions with AlphaFold 3. *Nature* **2024,** *630*, 493–500. Addendum: Accurate structure prediction of biomolecular interactions with AlphaFold 3. *Nature* **2024,** *636*, E4. Corresponding to reference 30 in the main text.
11. Lee, H. J.; Hota, P. K.; Chugha, P.; Guo, H.; Miao, H.; Zhang, L.; Kim, S. J.; Stetzik, L.; Wang, B. C.; Buck, M. NMR structure of a heterodimeric SAM:SAM complex: characterization and manipulation of EphA2 binding reveal new cellular functions of SHIP2. *Structure* **2012,** *20*, 41–55. Corresponding to reference 14 in the main text.
12. Waterhouse, A.; Bertoni, M.; Bienert, S.; Studer, G.; Tauriello, G.; Gumienny, R.; Heer, F. T.; de Beer, T. A. P.; Rempfer, C.; Bordoli, L.; Lepore, R.; Schwede, T. SWISS-MODEL: homology modelling of protein structures and complexes. *Nucleic Acids Res.* **2018,** *46*, W296–W303. Corresponding to reference 32 in the main text.
13. Meng, E. C.; Goddard, T. D.; Pettersen, E. F.; Couch, G. S.; Pearson, Z. J.; Morris, J. H.; Ferrin, T. E. UCSF ChimeraX: Tools for structure building and analysis. *Protein Sci.* **2023,** *32*, e4792. Corresponding to reference 124 in the main text.
14. Koradi, R.; Billeter, M.; Wuthrich, K. MOLMOL: a program for display and analysis of macromolecular structures. *J. Mol. Graph.* **1996,** *14*, 51–5, 29–32. Corresponding to reference 106 in the main text.
15. de Vries, S. J.; van Dijk, M.; Bonvin, A. M. The HADDOCK web server for data-driven biomolecular docking. *Nat. Protoc.* **2010,** *5*, 883–97. Corresponding to reference 20 in the main text.
16. Uniprot Consortium. UniProt: the Universal Protein Knowledgebase in 2023. *Nucleic Acids Res.* **2023,** *51*, D523–D531. Corresponding to reference 21 in the main text.
17. Laskowski, R. A.; Swindells, M. B. LigPlot+: multiple ligand-protein interaction diagrams for drug discovery. *J. Chem. Inf. Model.* **2011,** *51*, 2778–86. Corresponding to reference 22 in the main text.
18. Wallace, A. C.; Laskowski, R. A.; Thornton, J. M. LIGPLOT: a program to generate schematic diagrams of protein-ligand interactions. *Protein Eng.* **1995,** *8*, 127–34. Corresponding to reference 23 in the main text.
19. Magana, P.; Kovalevskiy, O. EMBL-EBI training course. Online Tutorial. AlphaFold: A Practical Guide. PAE: A measure of global confidence in AlphaFold2 predictions. In AlphaFold a practical guide. https://www.ebi.ac.uk/training/online/courses/alphafold/inputs-and-outputs/evaluating-alphafolds-predicted-

structures-using-confidence-scores/pae-a-measure-of-global-confidence-in-alphafold-predictions/ (01/09/2026). Corresponding to reference 103 in the main text.
20. Xia, Y.; Zhao, K.; Liu, D.; Zhou, X.; Zhang, G. Multi-domain and complex protein structure prediction using inter-domain interactions from deep learning. *Commun. Biol.* **2023,** *6*, 1221. Corresponding to reference 104 in the main text.